THE JOURNAL OF BIOLOGICAL CHEMISTRY VOL. 291, NO. 16, pp. 8721–8734, April 15, 2016

The B3 Subunit of the Cone Cyclic Nucleotide-gated Channel Regulates the Light Responses of Cones and Contributes to the Channel Structural Flexibility*

Received for publication, October 3, 2015, and in revised form, February 16, 2016 Published, JBC Papers in Press, February 18, 2016, DOI 10.1074/jbc.M115.696138

Xi-Qin Ding[‡1], Arjun Thapa[‡2], Hongwei Ma[‡], Jianhua Xu[‡3], Michael H. Elliott[§¶], Karla K. Rodgers[‖], Marci L. Smith[**], Jin-Shan Wang[‡‡], Steven J. Pittler[**], and Vladimir J. Kefalov[‡‡]

From the Departments of [‡]Cell Biology and [§]Ophthalmology and [‖]Biochemistry, University of Oklahoma Health Sciences Center and [¶]Dean McGee Eye Institute, Oklahoma City, Oklahoma 73104, [**]Department of Vision Sciences, University of Alabama, Birmingham, Alabama 35924, and [‡‡]Department of Ophthalmology and Visual Sciences, Washington University School of Medicine, Saint Louis, Missouri 63110

Cone photoreceptor cyclic nucleotide-gated (CNG) channels play a pivotal role in cone phototransduction, which is a process essential for daylight vision, color vision, and visual acuity. Mutations in the cone channel subunits CNGA3 and CNGB3 are associated with human cone diseases, including achromatopsia, cone dystrophies, and early onset macular degeneration. Mutations in CNGB3 alone account for 50% of reported cases of achromatopsia. This work investigated the role of CNGB3 in cone light response and cone channel structural stability. As cones comprise only 2–3% of the total photoreceptor population in the wild-type mouse retina, we used *Cngb3*$^{-/-}$/*Nrl*$^{-/-}$ mice with CNGB3 deficiency on a cone-dominant background in our study. We found that, in the absence of CNGB3, CNGA3 was able to travel to the outer segments, co-localize with cone opsin, and form tetrameric complexes. Electroretinogram analyses revealed reduced cone light response amplitude/sensitivity and slower response recovery in *Cngb3*$^{-/-}$/*Nrl*$^{-/-}$ mice compared with *Nrl*$^{-/-}$ mice. Absence of CNGB3 expression altered the adaptation capacity of cones and severely compromised function in bright light. Biochemical analysis demonstrated that CNGA3 channels lacking CNGB3 were more resilient to proteolysis than CNGA3/CNGB3 channels, suggesting a hindered structural flexibility. Thus, CNGB3 regulates cone light response kinetics and the channel structural flexibility. This work advances our understanding of the biochemical and functional role of CNGB3 in cone photoreceptors.

* This work was supported by grants from the National Center for Research Resources (P20RR017703), the National Eye Institute (P30EY021725, T32EY023202, EY019490 (X. Q. D.), EY019494 (M. H. E.), AI-094141 (K. K. R.), EY018143 (S. J. P.), EY003039 (S. J. P.), EY019312 (V. J. K.), EY021126 (V. J. K.), and EY002687 to the Department of Ophthalmology and Visual Sciences at Washington University), the Research to Prevent Blindness, and the Oklahoma Center for the Advancement of Science and Technology. The authors declare that they have no conflicts of interest with the contents of this article. The content is solely the responsibility of the authors and does not necessarily represent the official views of the National Institutes of Health.

[1] To whom correspondence should be addressed: Dept. of Cell Biology, University of Oklahoma Health Sciences Center, 940 Stanton L. Young Blvd., BMSB 553, Oklahoma City, OK 73104. Tel.: 405-271-8001 (ext. 47966); Fax: 405-271-3548; E-mail: xi-qin-ding@ouhsc.edu.

[2] Present address: Dept. of Chemical and Nuclear Engineering, Center for Biomedical Engineering, University of New Mexico, Albuquerque, NM 87131.

[3] Present address: Inst. of Reproduction and Development/ Insts. of Biomedical Sciences, Fudan University, 2140 Xietu Rd., Shanghai, China 200032.

The cone cyclic nucleotide-gated (CNG)[4] channels are localized to the plasma membrane of the photoreceptor outer segments and play an essential role in cone phototransduction. In darkness/dim light, the cone channels are kept opened by cyclic guanosine monophosphate (cGMP), maintaining a steady inward current of sodium and calcium. Light induces hydrolysis of cGMP, resulting in closure of the channels and hyperpolarization of the cell (1–3). The cone CNG channels belong to the superfamily of pore-loop cation channels. They share a common domain structure with hyperpolarization-activated cyclic nucleotide-gated channels and Eag-like K^+ channels (3–5). The channel comprises two structurally related subunits, CNGA3 and CNGB3. Mutations in genes encoding CNGA3 and CNGB3 are associated with achromatopsia and cone dystrophies (6–9). Mutations in CNGB3 alone account for over 50% of all known cases of achromatopsia (9–11). Mutations in CNGB3 have also been found in canine models of achromatopsia (12–14). Achromatopsia is an inherited disorder that affects ~1 in every 33,000 Americans. The condition is characterized by an inability to distinguish colors, impaired visual acuity, photophobia/hemeralopia, and pendular nystagmus. As the disease is primarily caused by mutations in the cone CNG channel subunits, achromatopsia is often referred to as a "channelopathy" (15).

CNGA3 and CNGB3 function as heterotetrameric complexes with CNGA3 acting as an ion-conducting subunit and CNGB3 serving as a modulator (16–20). In a heterologous expression system, CNGA3 forms a functional channel, whereas CNGB3 does not form channels in the absence of CNGA3. However, co-expressed CNGA3 and CNGB3 form heteromeric channels functionally similar to typical native CNG channels (16, 21). Using mouse retinas, we previously demonstrated the interaction between CNGB3 and CNGA3 and the nature of the tetrameric channel complexes in mammalian cones (22). The essential role of CNGB3 was shown in *Cngb3*$^{-/-}$ (rod-dominant) and *Cngb3*$^{-/-}$/*Nrl*$^{-/-}$ (cone-dom-

[4] The abbreviations used are: CNG, cyclic nucleotide-gated; CAR, cone arrestin; D-AP5, D-2-amino-5-phosphonovalerate; ERG, electroretinogram; GNAT2, guanine nucleotide-binding protein subunit α-2; L-AP4, L-(+)-2-amino-4-phosphonobutyric acid; NBQX, 2,3-dioxo-6-nitro-1,2,3,4-tetrahydrobenzo[*f*]quinoxaline-7-sulfonamide; NRL, neural retina leucine zipper; P, postnatal day; TPCK, L-1-tosylamido-2-phenylethyl chloromethyl ketone; cd, candela; t_p, time to peak; t_{rec}, recovery time constant; 8-pCPT-cGMP, 8-(4-chlorophenylthio)-guanosine 3′,5′-cyclic monophosphate.

inant) mice. These mice display impaired cone light response and early onset, progressive cone degeneration (23–25), resembling human patients with *CNGB3* mutations.

The present work investigates the functional properties of cones lacking CNGB3 and the biochemical features of CNG channel complexes lacking CNGB3 to understand the role of CNGB3 in cones. To facilitate the analysis of biochemical properties of the cone channels and light response properties of the mouse cones, we used cone-dominant $Cngb3^{-/-}/Nrl^{-/-}$ mice. We show that CNGB3 regulates the cone light response and channel structural flexibility. CNGB3-deficient cones show impaired photopic a-wave and b-wave responses, altered light adaptation, and compromised ability to function in bright light. CNGA3 channels lacking CNGB3 are more resilient to proteolytic digestion than CNGA3/CNGB3 channels. Moreover, the C terminus of CNGA3 in the absence of the C terminus of CNGB3 shows a more dramatic circular dichroism (CD) profile alteration in response to cGMP. This work provides insights into the biochemical and functional role of CNGB3 in cone photoreceptors.

Experimental Procedures

Mice, Antibodies, and Other Materials—Wild-type C57BL/6J mice were purchased from The Jackson Laboratory (Bar Harbor, ME). The $Cngb3^{-/-}$ (23), $Cngb1^{-/-}$ (26), $Nrl^{-/-}$ (27) (kindly provided by Dr. Anand Swaroop, National Eye Institute, National Institutes of Health), and $Cngb3^{-/-}/Nrl^{-/-}$ (24, 28) mouse lines were generated as described previously. NRL is a basic motif neural retina leucine zipper transcription factor essential for the normal development of rods. Mice lacking the *Nrl* gene have no rods but have increased numbers of S-cones, functionally manifested as a loss of rod function coupled with supernormal cone function (27, 29). Morphologically, $Nrl^{-/-}$ retinas have a conelike nucleus, short and disorganized outer segments, and a rosette-like structure (27, 29). As a unique mammalian cone-dominant model, the $Nrl^{-/-}$ mouse line has been commonly used to study cone biology and disease (22, 24, 28, 30–33). We previously showed that the retinas of $Nrl^{-/-}$ mice express an abundant amount of cone CNG channel and lack the expression of the rod channel (22). We also showed that $Cngb3^{-/-}/Nrl^{-/-}$ mice have a retinal phenotype similar to that of $Cngb3^{-/-}$ mice, that is impaired cone function and cone apoptosis/degeneration (24, 28).

Mice at ages between postnatal day 30 (P30) and 40 were used for functional and biochemical evaluations, except those used in the age-dependent cone light response study. All mice were maintained under cyclic light (12-h light-dark) conditions. During the light cycle, cage illumination was ~75 lux. All animal maintenance and experiments were approved by the local Institutional Animal Care and Use Committees (University of Oklahoma Health Sciences Center, Oklahoma City, OK, and Washington University, Saint Louis, MO) and conformed to the guidelines on the care and use of animals adopted by the Society for Neuroscience (Washington, D. C.) and the Association for Research in Vision and Ophthalmology (Rockville, MD).

Rabbit antibodies against mouse CNGA3 and CNGB3 were generated against peptides corresponding to the sequence between residues 77 and 97 (SNAQPNPGEQKPPDGGEGRKE) of mouse CNGA3 and a region between residues 677 and 694 (CKVDLGRLLKGKRKTTTQK) of mouse CNGB3 as described previously (22, 34). Rabbit anti-M-opsin and anti-cone arrestin (CAR) were provided by Dr. Cheryl Craft (University of Southern California Keck School of Medicine). Rabbit anti-S-opsin was supplied by Dr. Muna Naash (University of Houston). Mouse monoclonal anti-CNGB1/glutamic acid-rich protein was provided by Dr. Robert Molday (University of British Columbia). Goat anti-S-opsin antibody (catalog number sc-14365) and rabbit anti-guanine nucleotide-binding protein subunit α-2 (GNAT2) antibody (catalog number sc-390) were purchased from Santa Cruz Biotechnology, Inc. (Dallas, TX). Mouse anti-β-actin (catalog number ab-6276) was obtained from Abcam (Cambridge, MA). Horseradish peroxidase (HRP)-conjugated anti-rabbit and anti-mouse secondary antibodies were procured from Kirkegaard and Perry Laboratories, Inc. (Gaithersburg, MD). Fluorescent goat anti-rabbit and donkey anti-goat antibodies were obtained from Invitrogen. Cross-linker bis(sulfosuccinimidyl)suberate was purchased from Pierce, and trypsin-TPCK was acquired from Worthington. L-(+)-2-amino-4-phosphonobutyric acid (L-AP4), D-2-amino-5-phosphonovalerate (D-AP5), and 2,3-dioxo-6-nitro-1,2,3,4-tetrahydrobenzo[*f*]quinoxaline-7-sulfonamide (NBQX) were procured from R&D Systems (Minneapolis, MN). All other reagents were purchased from Sigma-Aldrich, Bio-Rad, and Life Technologies.

Retinal Membrane Protein Preparation, SDS-PAGE, and Western Blotting Analysis—Mouse retinas were homogenized in homogenization buffer consisting of 20 mM HEPES-NaOH, pH 7.4, 1 mM EDTA, and 200 mM sucrose containing protease inhibitor mixture (Sigma-Aldrich) (25). The homogenate was centrifuged at 1,000 × *g* for 10 min at 4 °C to pellet down nuclei and cell debris. The supernatant of the homogenate was further centrifuged at 16,000 × *g* for 30 min at 4 °C to separate out membrane fractions followed by protein concentration quantifications using the Bradford assay (Bio-Rad). The resulting membrane proteins were then solubilized in SDS-PAGE sample buffer, separated by 10% SDS-PAGE, and transferred onto a polyvinylidene difluoride membrane (PVDF) (Bio-Rad). After 1 h of blocking in 5% milk containing Tris-buffered saline with 0.1% Tween (v/v; TBST) at room temperature, the membranes were incubated with primary antibodies overnight at 4 °C (anti-CNGA3, 1:250; anti-CNGB3, 1:250; anti-M-opsin, 1:2,000; anti-CAR, 1:2,000; anti-GNAT2, 1:500; anti-CNGB1, 1:50; and anti-β-actin, 1:2,000). The membranes were then washed with TBST three times and incubated with HRP-conjugated secondary anti-rabbit or anti-mouse for 1 h at room temperature. After washing, antigen and antibody binding was detected using the SuperSignal® West Dura Extended Duration chemiluminescent substrate (Pierce). The blots were scanned, and images were captured using a Kodak Image Station 4000R Digital Imaging System (Carestream Molecular Imaging, New Haven, CT) or were developed using HyBlot CL autoradiography films (Denville Scientific, Inc., Metuchen, NJ). Densitometry analysis was performed by quantifying the intensities of the bands of interest using Kodak Molecular Imaging software or Adobe Photoshop CS5 as described previously (35, 36). Actin was used as a loading control. The linearity of actin detection with total

protein loaded in each lane, detected by Coomassie R350 (GE Healthcare, catalog number 17-0518-01) staining, was confirmed in the mouse retina (data not shown). The densitometric measurements were analyzed and graphed using GraphPad Prism® software (GraphPad Software, San Diego, CA).

Eye Preparation, Immunofluorescence Labeling, and Confocal Microscopy—To prepare mouse eye cross-sections, euthanasia of mice was performed by CO_2 asphyxiation, and mouse eyes were enucleated and fixed with Prefer (Anatech Ltd., Battle Creek, MI) for 25–30 min at room temperature (23). The superior portion of the cornea was marked with a green dye for orientation before enucleation. Fixed eyes were then transferred in 70% ethanol and stored at 4 °C until processing. We prepared 5-μm-thick paraffin sections passing vertically through the retina along the vertical meridian passing through the optic nerve head using a Leica microtome (Leica Biosystems, Buffalo Grove, IL). For immunofluorescence labeling, eye sections were deparaffinized, rehydrated, and blocked with PBS containing 5% BSA and 0.5% Triton X-100 for 1 h at room temperature (23). Antigen retrieval was performed by incubating tissues in 10 mM sodium citrate buffer, pH 6.0, for 30 min in a 70 °C water bath. Primary antibody incubation (anti-CNGA3, 1:250 and anti-S-opsin, 1:500) was performed at room temperature for 2 h. Co-immunofluorescence labeling was performed using rabbit anti-CNGA3 with goat anti-S-opsin. Following fluorescence-conjugated secondary antibody incubation and rinses, slides were mounted and coverslipped. Immunofluorescence signals were imaged using an Olympus FV1000 confocal laser scanning microscope (Olympus, Melville, NY) and FluoView imaging software (Olympus).

Chemical Cross-linking—These experiments were performed using retinal membrane preparations as described previously (22, 37). The amino-specific cross-linker bis(sulfosuccinimidyl)suberate (0.5 mM) was used as a biofunctional cross-linker. The time-dependent reactions were carried out by the addition of 500 mM Tris-HCl, pH 7.5, at 0.5, 3, and 30 min. Cross-linked products were resolved by 3–8% NuPAGE (Life Technologies) and analyzed by Western blotting with anti-CNGA3 antibody. Densitometry analysis was performed to quantify the intensities of the bands of the different channel complex species (*i.e.* monomers, dimers, trimers, and tetramers). For each cross-linking duration, the relative levels of different species (in percentage of the total levels) were analyzed and graphed.

Electrophysiological Recordings—For serial photopic ERG recordings, animals were anesthetized by intraperitoneal injection of 85 mg/kg ketamine and 14 mg/kg xylazine and light-adapted to 1.46 log cd s m^{-2} light for 5 min after overnight dark adaptation (23, 38). Afterward, a strobe flash was presented to the dilated eyes at increasing intensities (−1.57 to 2.40 log cd s m^{-2}) in the Ganzfeld. Responses were differentially amplified, averaged, and stored using a Nicolet Compact 4 signal averaging system. Photopic flicker ERG recordings were performed using an Espion Visual Electrophysiology System (Diagnosys LLC, Lowell, MA). In brief, animals were light-adapted for 10 min (50 cd m^{-2} background) after an overnight dark adaptation. Flicker ERGs were then recorded at 3-, 10-, 20-, and 30-Hz fusion frequency with white stimuli delivered by a xenon bulb (6500 K) at 4-ms duration and a 15-cd s m^{-2} intensity. Data were analyzed with Espion 100 software version 4.2006.818.51. Transretinal ERG recordings were performed from isolated retinas as described previously (39, 40). In retinas from the rod-dominant wild-type and *Cngb3*$^{-/-}$ mice, the rod component of the response was blocked by background light. In retinas from the cone-only *Nrl*$^{-/-}$ and *Cngb3*$^{-/-}$/*Nrl*$^{-/-}$ mice, recordings were performed in darkness. The inner retina response was blocked pharmacologically by a mixture of 10 mM barium chloride, 5 μM L-AP4, 50 μM D-AP5, and 5 μM NBQX as described previously (40). Test flashes (500 nm) of intensity increasing in 0.5-log unit steps and 20 ms in duration were delivered at $t = 0$. The maximal response was measured as the amplitude of the saturating flash response. Time to peak (t_p) was measured from the onset of the test flash to the peak of the dim flash response, and recovery time constant (t_{rec}) was estimated from the single exponential fit to the tail of the dim flash response. Flash sensitivity was estimated as the ratio of the dim flash response amplitude and the corresponding flash intensity. The stimulus producing half-maximal response ($I_{1/2}$) was estimated by fitting the intensity-response data with the Naka-Rushton function $R/R_{max} = (1 + I_{1/2}/I)^{-1}$ where R is the transient peak amplitude of the response, R_{max} is the maximal response amplitude, and I is the flash intensity. The photosensitivity under increasing background lights was plotted and fitted with the Weber-Fechner function $S/S_{DA} = (1 + I_B{}^k/I_0{}^k)^{-1}$ where S is the light-adapted sensitivity, S_{DA} is the dark-adapted sensitivity, I_B is the intensity of the background, I_0 is the background that reduced sensitivity to half of S_{DA}, and k is the Hill coefficient.

Trypsin-TPCK Digestion—Limited tryptic digestion experiments were performed as described previously (41, 42). Retinal membranes (40 μg of protein) were resuspended in protease inhibitor-free Tris buffer and incubated with trypsin-TPCK (30 μg/ml; at an approximate 1:6 ratio of trypsin-TPCK to membrane proteins) at 30 °C for 0.5, 2, and 5 min. The trypsin-treated samples were then solubilized with 2× Laemmli sample buffer and resolved by 10% SDS-PAGE followed by immunoblotting analysis using anti-CNGA3 and anti-CNGB3 antibodies. Densitometry analysis was performed to quantify the intensities of CNGA3 bands. For each genotype, the relative levels of CNGA3 remaining after different durations of digestion (in percentage of the control/time point 0 levels) were analyzed and graphed.

Velocity Sedimentation Analysis—Velocity sedimentation analysis of the channel complexes was performed using continuous density gradients of 5–20% sucrose (38, 43). Mouse retinas were homogenized in Tris buffer containing 20 mM Tris acetate, pH 7.2, 0.25 mM $MgCl_2$, 8 mM taurine, 8 mM D-glucose, 20% (w/v) sucrose, and protease mixture (Sigma-Aldrich) at 4 °C. Photoreceptor outer segments were dislodged by vigorous vortexing (3 × 30s), collected after centrifugation at 2,500 × *g* for 1 min, and solubilized in PBS containing 2% Triton X-100 and 2 mM DTT, pH 7.5. The solubilized outer segment proteins were loaded onto 5–20% sucrose gradients followed by centrifugation at 250,000 × *g* for 16 h at 4 °C, and 0.5-ml fractions were collected from the top of the gradients and subjected to 10% SDS-PAGE and Western blotting analysis with anti-CNGA3 antibody. Densitometry analysis was performed to quantify the

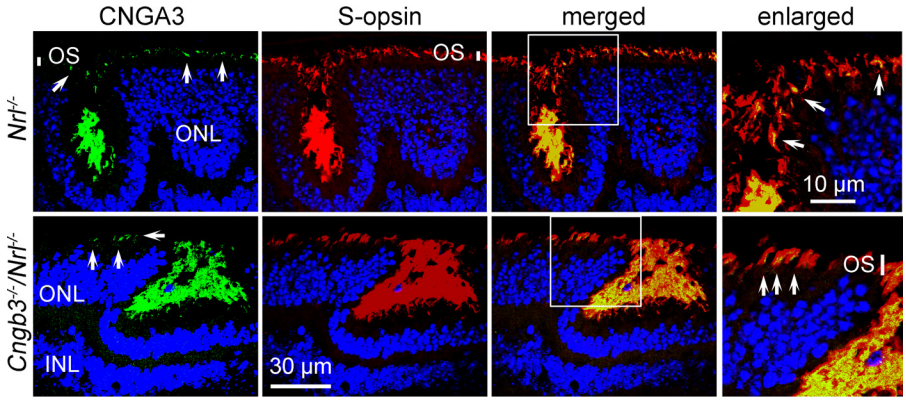

FIGURE 1. **CNGA3 is localized to the cone outer segments of *Cngb3*$^{-/-}$/*Nrl*$^{-/-}$ retinas.** Co-immunofluorescence labeling of CNGA3 with S-opsin was performed on retinal sections from P30 *Nrl*$^{-/-}$ and *Cngb3*$^{-/-}$/*Nrl*$^{-/-}$ mice. Shown are representative confocal images of the co-labeling of CNGA3 with S-opsin. *Arrows* annotate the localization of CNGA3 in the outer segments. *OS*, outer segment; *ONL*, outer nuclear layer; *INL*, inner nuclear layer.

intensities of CNGA3 bands. For each genotype, the relative levels of CNGA3 present in each fraction (in percentage of the total of all fractions) were analyzed and graphed.

Circular Dichroism Spectropolarimetry—Expression and purification of the glutathione *S*-transferase (GST) fusion CNGA3 (amino acids 340–631) and CNGB3 (amino acids 432–694) C termini were performed as we described previously (41). The concentration of purified fusion proteins was quantified with the Bradford assay using BSA as the standard and by UV absorbance at 280 nm. Expression of the fusion proteins was also examined by Coomassie Blue staining and by Western blotting using anti-GST (Amersham Biosciences) and anti-CNGA3 and anti-CNGB3 antibodies. The CD spectroscopy experiments were performed using a Jasco J715 spectropolarimeter with a PTC-348WI Peltier temperature controller (Jasco, Tokyo, Japan) as we described previously (41). Protein samples were dialyzed against PBS, pH 7.4, containing 2 mM KH_2PO_4, 10 mM $Na_2HPO_47H_2O$, 137 mM NaCl, and 2.7 mM KCl at 4 °C overnight prior to CD spectropolarimetry analysis. Spectra were obtained from 5 μM protein with the wavelength ranging from 250 to 200 nm using 0.1-cm cuvette path length at 25 °C, and the results were expressed as the mean molar ellipticity. The cGMP analog 8-pCPT-cGMP (100 μM) (Sigma-Aldrich) was used to examine the conformational changes of the channel subunit C termini in response to the ligand. Thermal denaturation curves were obtained at 220 nm from 20 to 80 °C.

Statistics—Results are expressed as means ± S.E. of the number (n) of observations. Student's t test was used to test for differences between two groups of data. Two-way analysis of variance was performed to evaluate significance of difference between genotypes at different ages. Differences were considered statistically significant when p was <0.05. All tests were performed using GraphPad Prism software.

Results

CNGA3 Localizes to the Outer Segments of Cngb3$^{-/-}$/*Nrl*$^{-/-}$ *Cones*—We previously reported that CNGA3 and CNGB3 are localized to the cone outer segments of rod-dominant wild-type and cone-only *Nrl*$^{-/-}$ retinas (22). Here, we sought to determine whether the targeting of CNGA3 is affected by deletion of CNGB3 by examining the cellular localization of CNGA3 in CNGB3-deficient cones. Due to the low expression level of CNGA3 in *Cngb3*$^{-/-}$ mice (23) and the sparse amount of cones in rod-dominant background mice, the experiments were performed with all-cone background *Cngb3*$^{-/-}$/*Nrl*$^{-/-}$ mice. We used cone opsin, which has been shown to localize to the outer segments both outside and inside the rosettes of *Nrl*$^{-/-}$ mice (27, 31), to identify cone outer segments. Co-immunofluorescence labeling using anti-CNGA3 and anti-S-opsin was performed on retinal sections prepared from *Nrl*$^{-/-}$ and *Cngb3*$^{-/-}$/*Nrl*$^{-/-}$ mice. Similar to that in *Nrl*$^{-/-}$ mice, CNGA3 immunoreactivity was detected in the outer segments and rosette-like structures in *Cngb3*$^{-/-}$/*Nrl*$^{-/-}$ mice co-localized with S-opsin (Fig. 1). Thus, the deletion of CNGB3 did not abolish the localization of CNGA3 to the outer segments.

CNGA3 Forms a Tetrameric Complex in Cngb3$^{-/-}$/*Nrl*$^{-/-}$ *Retinas*—Using chemical cross-linking, anti-CNGA3 and anti-CNGB3 antibodies, and *Nrl*$^{-/-}$ retinas, we previously demonstrated the nature of the tetrameric complexes of the cone CNG channel comprising CNGA3 and CNGB3 in the mouse retina (22). In the current work, we examined the channel complex formation in *Cngb3*$^{-/-}$/*Nrl*$^{-/-}$ retinas using the same methods. We first examined expression levels of CNGA3 in *Cngb3*$^{-/-}$/*Nrl*$^{-/-}$ retinas. Similar to that in *Cngb3*$^{-/-}$ mice (23), the expression level of CNGA3 was significantly lower in *Cngb3*$^{-/-}$/*Nrl*$^{-/-}$ retinas than that in *Nrl*$^{-/-}$ retinas (Fig. 2*A*). However, its reduction in *Cngb3*$^{-/-}$/*Nrl*$^{-/-}$ mice (~45%) was lesser compared with *Cngb3*$^{-/-}$ mice (~80%). Chemical cross-linking was performed using retinal membranes prepared from *Cngb3*$^{-/-}$/*Nrl*$^{-/-}$ and *Nrl*$^{-/-}$ mice. Following cross-linking reactions, the cross-linked products equivalent to the dimer (~150 kDa), trimer (~240 kDa), and tetramer (~320 kDa) of the channel were detected by anti-CNGA3 antibody in *Cngb3*$^{-/-}$/*Nrl*$^{-/-}$ retinas as they were in *Nrl*$^{-/-}$ retinas (Fig. 2*B*). Among the varying species of the channel complexes detected after cross-linking reaction, the tetramers in *Nrl*$^{-/-}$ mice represented about 50% of the total signals, whereas the tetramers in *Cngb3*$^{-/-}$/*Nrl*$^{-/-}$ mice were only about 7% of the total signals (Fig. 2*B*, *lower panel*, *d*). Of note, a relatively large amount of the trimers was detected in *Cngb3*$^{-/-}$/*Nrl*$^{-/-}$ mice compared with *Nrl*$^{-/-}$ mice (Fig. 2*B*), suggesting a relative abundance of CNGA3 trimers in the absence of CNGB3. Thus, despite the absence of CNGB3 and its reduced expression, CNGA3

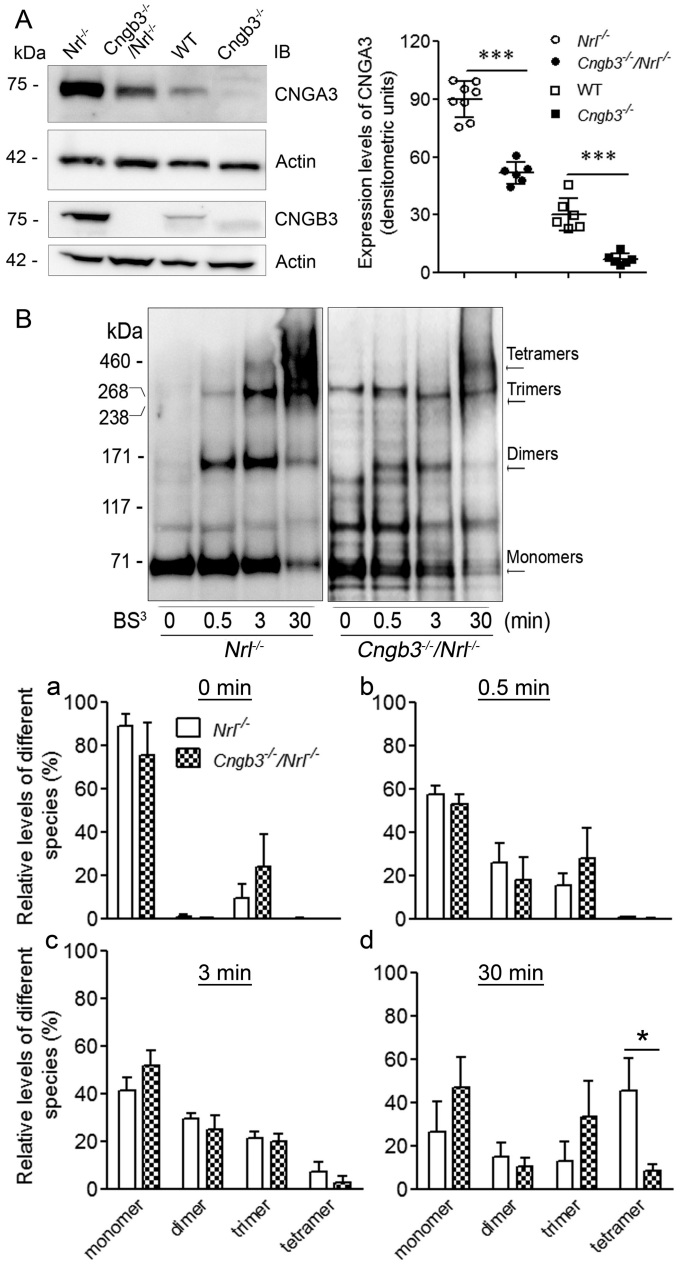

FIGURE 2. **CNGA3 forms tetrameric complexes in *Cngb3*$^{-/-}$/*Nrl*$^{-/-}$ retinas.** *A*, immunoblotting (*IB*) detection of CNGA3 and CNGB3 expression in P30 *Nrl*$^{-/-}$, *Cngb3*$^{-/-}$/*Nrl*$^{-/-}$, wild-type (*WT*), and *Cngb3*$^{-/-}$ retinas. Shown are representative images of the Western blotting detections (*left panel*) and the corresponding densitometric analyses (*right panel*). *B*, detection of CNGA3 homotetrameric complexes in *Cngb3*$^{-/-}$/*Nrl*$^{-/-}$ retinas. Chemical cross-linking was performed using the amino-specific cross-linker bis(sulfosuccinimidyl)suberate (*BS*^{3}) on retinal membranes prepared from P30 *Nrl*$^{-/-}$ and *Cngb3*$^{-/-}$/*Nrl*$^{-/-}$ mice at varying durations as indicated. The cross-linking products were separated by 3–8% NuPAGE followed by immunoblotting using anti-CNGA3 antibody. Shown are representative images of the Western blotting detections (*upper panel*) and the corresponding densitometric analyses (*lower panel*, *a–d*). Data are represented as mean ± S.E. from three assays using retinas prepared from eight to 10 mice. Unpaired Student's *t* test was used to determine the significances of differences (*, $p < 0.05$; ***, $p < 0.001$). *Error bars* represent S.E.

appeared to be able to form tetrameric complexes by itself in cones. However, the relative amount of the tetramers was significantly reduced in *Cngb3*$^{-/-}$/*Nrl*$^{-/-}$ mice compared with that in *Nrl*$^{-/-}$ mice.

Reduced Photopic Light Response in Cngb3$^{-/-}$ *and Cngb3*$^{-/-}$/*Nrl*$^{-/-}$ *Mice*—To begin analyzing the effects of CNGB3 deletion on cone function, we first examined the photopic light responses in *Cngb3*$^{-/-}$/*Nrl*$^{-/-}$ mice. Characterizing the photopic a-wave response, which primarily reflects the responsiveness of cone photoreceptors, is difficult due to its small amplitude in rod-dominant mice. As a result, the photopic b-wave responses are commonly used to estimate the function of cones in mice (27, 31, 38, 44, 45). However, the a-wave in the all-cone *Nrl*$^{-/-}$ retina is larger and can be measured directly (Fig. 3, *A* and *B*). This allowed us to evaluate directly the effect of CNGB3 deletion on cone function by comparing the a-wave responses in *Nrl*$^{-/-}$ and *Cngb3*$^{-/-}$/*Nrl*$^{-/-}$ mice. We found that the a-wave responses were dramatically reduced in P30 *Cngb3*$^{-/-}$/*Nrl*$^{-/-}$ mice (Fig. 3, *A* and *B*). The a-wave responses at high flash intensities (1.89–2.40 log cd s m^{-2}) were reduced by about 80% in *Cngb3*$^{-/-}$/*Nrl*$^{-/-}$ mice compared with those in age-matched *Nrl*$^{-/-}$ controls (Fig. 3*B*, *upper panel*). Consistent with this, the calculated $I_{1/2}$ values in *Nrl*$^{-/-}$ and *Cngb3*$^{-/-}$/*Nrl*$^{-/-}$ mice were 10.1 ± 3.3 and 51.4 ± 24.9 cd s m^{-2}, respectively, and the asymptotic maximal amplitudes of the response were 184.0 ± 18.3 and 32.9 ± 8.9 μV, respectively. Similar to *Cngb3*$^{-/-}$ mice (25), the photopic b-wave responses in *Cngb3*$^{-/-}$/*Nrl*$^{-/-}$ mice were significantly impaired. The b-wave responses at high flash intensities were reduced by about 40% in *Cngb3*$^{-/-}$/*Nrl*$^{-/-}$ mice compared with those in age-matched *Nrl*$^{-/-}$ controls (Fig. 3*B*, *lower panel*). The calculated $I_{1/2}$ values in *Nrl*$^{-/-}$ and *Cngb3*$^{-/-}$/*Nrl*$^{-/-}$ mice were 4.8 ± 0.6 and 37.3 ± 12.6 cd s m^{-2}, respectively, and the asymptotic maximal amplitudes of the response were 983.3 ± 46.5 and 634.7 ± 126.8 μV, respectively. These data demonstrate a reduced cone response and cone-mediated secondary neuron response in the absence of CNGB3.

ERG responses elicited by flickering light stimuli at a series of pulses provide information on the temporal processing properties of phototransduction (46, 47). We measured flicker ERG responses of P30 *Nrl*$^{-/-}$, *Cngb3*$^{-/-}$/*Nrl*$^{-/-}$, wild-type, and *Cngb3*$^{-/-}$ mice under photopic conditions with a frequency range from 3 to 30 Hz (47) using the Espion Visual Electrophysiology System. As shown in Fig. 3*C*, the responses in *Cngb3*$^{-/-}$ and *Cngb3*$^{-/-}$/*Nrl*$^{-/-}$ mice were significantly diminished compared with their respective controls. Thus, the deletion of CNGB3 may reduce the temporal resolution of cone-driven flicker ERG responses. We next sought to determine whether this flicker deficiency is caused by abnormal cone response shutoff in the absence of CNGB3.

Impaired Light Response Kinetics in Cngb3$^{-/-}$ *and Cngb3*$^{-/-}$/*Nrl*$^{-/-}$ *Retinas*—To investigate directly the effect of CNGB3 deletion on cone function, we examined the cone light responses in *Cngb3*$^{-/-}$ and *Cngb3*$^{-/-}$/*Nrl*$^{-/-}$ mice with transretinal ERG recordings. This method allows investigation of the cone sensitivity, response kinetics, maximal response amplitude, and phototransduction adaptation in *ex vivo* conditions (48, 49). The cone component of the response in rod-dominant wild-type and *Cngb3*$^{-/-}$ mice was obtained by saturating the rods with background light. The responses from the all-cone *Nrl*$^{-/-}$ and *Cngb3*$^{-/-}$/*Nrl*$^{-/-}$ retinas were obtained in dark-adapted conditions. In both cases, the inner retina

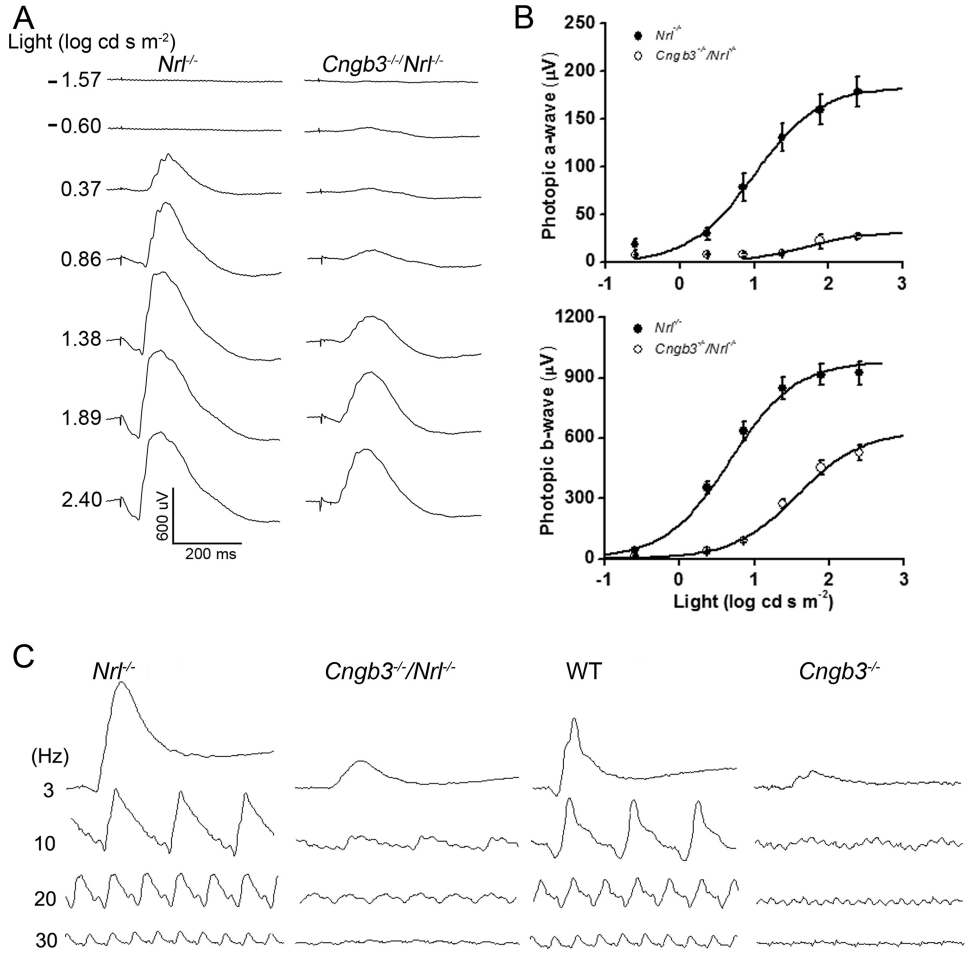

FIGURE 3. **Impaired photopic light response in *Cngb3*$^{-/-}$ and *Cngb3*$^{-/-}$/*Nrl*$^{-/-}$ mice.** *A* and *B*, reduced photopic ERG responses in *Cngb3*$^{-/-}$/*Nrl*$^{-/-}$ mice. Ganzfeld photopic ERG recordings were performed with serial stimuli at increasing intensities in P30 *Cngb3*$^{-/-}$/*Nrl*$^{-/-}$ and *Nrl*$^{-/-}$ mice. Shown are representative waveforms (*A*) and a/b-wave amplitude quantifications of the light responses fit with the Naka-Rushton function (*B*). Data are represented as mean ± S.E. of three independent measurements from four to six mice. *C*, impaired photopic flicker ERG response in *Cngb3*$^{-/-}$ and *Cngb3*$^{-/-}$/*Nrl*$^{-/-}$ mice. Flicker ERG recordings were performed with P30 wild-type (*WT*), *Cngb3*$^{-/-}$, *Nrl*$^{-/-}$, and *Cngb3*$^{-/-}$/*Nrl* mice under photopic conditions in the frequency range from 3 to 30 Hz. Shown are representative waveforms of the flicker recordings. Data are represented as mean ± S.E. of three independent measurements from six to 10 mice. *Error bars* represent S.E.

response was blocked pharmacologically using L-AP4, NBQX, and D-AP5 (see "Experimental Procedures" for details). Comparison of the cone-driven responses in wild-type and *Cngb3*$^{-/-}$ mice revealed a substantially reduced maximal cone response amplitude, lower sensitivity, and abnormally slow recovery kinetics (Fig. 4*A*). The removal of CNGB3 produced similar effects on the photoresponses in the all-cone *Nrl*$^{-/-}$ background (Fig. 4*B*): the maximum response amplitude in *Cngb3*$^{-/-}$/*Nrl*$^{-/-}$ retinas decreased about 3-fold, dim flash sensitivity was reduced 8.2-fold from 5.3 ± 0.6 × 10^{-4} to 6.5 ± 1.2 × 10^{-5} μV photons^{-1} μm^2, and response kinetics were slower with t_p increasing from 66 ± 15 to 108 ± 19 ms and t_{rec} increasing from 54 ± 16 to 175 ± 32 ms in *Nrl*$^{-/-}$ (n = 12) and *Cngb3*$^{-/-}$/*Nrl*$^{-/-}$ (n = 8) retinas, respectively. Thus, consistent with our results from *in vivo* ERG recordings above, the deletion of CNGB3 dramatically affected the cone photoresponse amplitude and sensitivity. Furthermore, the dramatically slower photoresponses of CNBG3-deficient cones explains the inability of the mutant mice to track high flicker stimulation.

Altered Background Adaptation and Functional Range in Cngb3$^{-/-}$/*Nrl*$^{-/-}$ *Retinas*—We next used transretinal ERG recordings to determine the effect of CNGB3 deletion on phototransduction adaptation by comparing the cone light adaptation capability and functional range in *Nrl*$^{-/-}$ and *Cngb3*$^{-/-}$/*Nrl*$^{-/-}$ retinas. The photosensitivity under increasing background light was plotted and fitted with the Weber-Fechner function (see "Experimental Procedures" for details). Fig. 5*A* shows the normalized sensitivity during background adaptation for *Nrl*$^{-/-}$ and *Cngb3*$^{-/-}$/*Nrl*$^{-/-}$ mice. Based on the 8.2-fold lower dark-adapted sensitivity of *Cngb3*$^{-/-}$/*Nrl*$^{-/-}$ cones, we expected that their adaptation curve would be shifted to correspondingly brighter light compared with *Nrl*$^{-/-}$ controls. Instead, the CNGB3 deficiency resulted in a 21-fold shift of the adaptation curve to lower background light intensities with I_0 decreasing from 44,700 ± 3,700 to 2,100 ± 149 photons μm^{-2} s^{-1}. Consistent with this apparent adaptation deficiency, the Hill coefficient, k, also increased from 0.6 for *Nrl*$^{-/-}$ cones to 0.75 for *Cngb3*$^{-/-}$/*Nrl*$^{-/-}$ cones. Thus, the deletion of CNGB3 dramatically altered the adap-

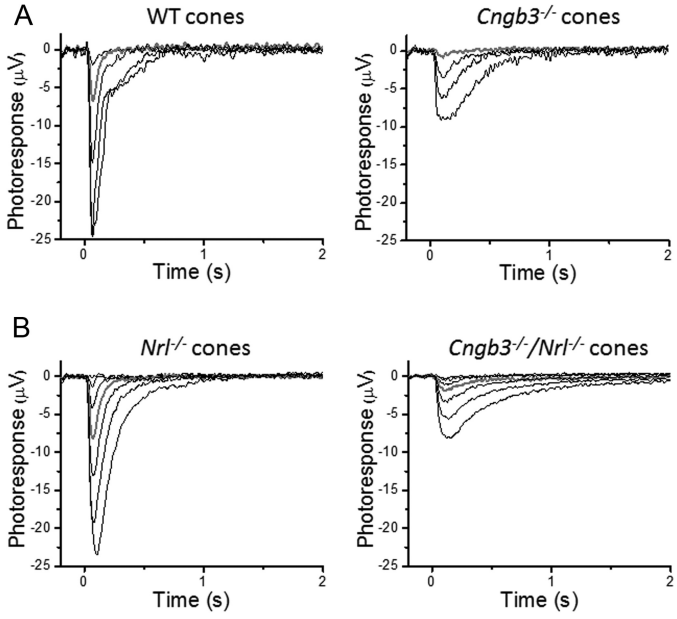

FIGURE 4. **Impaired cone light response kinetics in *Cngb3*$^{-/-}$ and *Cngb3*$^{-/-}$/*Nrl*$^{-/-}$ mice.** Transretinal ERG recordings were performed in retinas from P30 wild-type (*WT*), *Cngb3*$^{-/-}$, *Nrl*$^{-/-}$, and *Cngb3*$^{-/-}$/*Nrl*$^{-/-}$ mice. *A*, representative families of cone-driven photoresponses recorded from wild-type (*left panel*) and *Cngb3*$^{-/-}$ (*right panel*) retinas in background light that saturated the rods. *B*, representative families of cone photoresponses recorded from *Nrl*$^{-/-}$ (*left panel*) and *Cngb3*$^{-/-}$/*Nrl*$^{-/-}$ (*right panel*) retinas in dark-adapted conditions. *Gray* traces represent photoresponses induced by a flash with the same intensity in all cases.

tation capacity of cones and compromised their ability to function in bright light.

We also investigated how strongly the regulatory B subunit of the CNG channel modulates background adaptation in cones *versus* rods. To do that, we compared the effect of CNGB3 deletion on cone function with the effect of deleting the rod channel B subunit (CNGB1a) and associated glutamic acid-rich proteins (26) on rod light adaptation. Similar to the cone channel, the rod channel comprises an ion-conducting subunit, CNGA1, and a modulatory subunit, CNGB1a. Mutations in genes encoding CNGA1 and CNGB1a cause retinitis pigmentosa (50). In dark-adapted conditions, the rod dim flash sensitivity of mice lacking CNGB1a (*Cngb1*$^{-/-}$) was 113-fold lower than that of wild-type controls ($6.7 \pm 0.9 \times 10^{-3}$ ($n = 8$) *versus* $7.6 \pm 0.5 \times 10^{-1}$ ($n = 16$) μV photon^{-1} μm^2). As expected from the lower dark-adapted sensitivity of the CNGB1a-deficient rods, their background adaptation curve was also shifted to brighter light compared with wild-type rods. However, despite the initial 113-fold lower dark-adapted sensitivity of CNGB1a-deficient rods, their corresponding background values for I_0 increased by only 10.5-fold from 456 ± 37 photons μm^{-2} s^{-1} for wild-type rods to $4{,}781 \pm 412$ photons μm^{-2} s^{-1} for *Cngb1*$^{-/-}$ rods (Fig. 5*B*). The Hill coefficient, *k*, also increased from 0.61 for wild-type rods to 0.73 for *Cngb1*$^{-/-}$ rods. Thus, the deletion of CNGB1a also altered the adaptation capacity of rods, but to a lower degree, compared with the corresponding effect of CNGB3 deletion in cones.

Age-dependent Reduction of the Photopic a-wave but Not the b-wave Responses in Cngb3$^{-/-}$/*Nrl*$^{-/-}$ *Mice*—To investigate whether the deletion of CNGB3 affects the long term function and survival of cones, we next examined the photopic light response in *Cngb3*$^{-/-}$/*Nrl*$^{-/-}$ mice at varying ages between 1 and 15 months compared with those in age-matched *Nrl*$^{-/-}$ mice. The a-wave and b-wave responses in *Nrl*$^{-/-}$ mice declined with age as has been reported previously (31, 51) (Fig. 6*A*). The a-wave response in *Cngb3*$^{-/-}$/*Nrl*$^{-/-}$ mice was reduced age-dependently up to 6 months compared with that in P30 mice (Fig. 6*A*, *left panel*). However, the b-wave response was largely preserved and stable in these mice (Fig. 6*A*, *right panel*). No significant reduction in the b-wave amplitude was observed up to 15 months compared with that in P30 mice. In comparison with age-matched *Nrl*$^{-/-}$ mice, the a-wave responses were ~ 5-fold lower in *Cngb3*$^{-/-}$/*Nrl*$^{-/-}$ mice at all ages examined except at 15 months (Fig. 6*A*, *left panel*). In contrast, the b-wave response in P30 *Cngb3*$^{-/-}$/*Nrl*$^{-/-}$ mice was reduced by only 50%; the difference between the two genotypes lessened at 3 months of age when the response was reduced by about 20%, and no difference was detected between the two genotypes at 6, 9, 12, or 15 months (Fig. 6*A*, *right panel*).

To evaluate any CNGB3 deficiency-associated cone degeneration, we examined the expression levels of cone-specific proteins, including CNGA3, CAR, GNAT2, and M-opsin, in 1- and 6-month *Cngb3*$^{-/-}$/*Nrl*$^{-/-}$ and *Nrl*$^{-/-}$ mice. Consistent with the gradual reduction in photopic ERG response above, we also found age-dependent decline in the protein expression levels in both *Cngb3*$^{-/-}$/*Nrl*$^{-/-}$ and *Nrl*$^{-/-}$ mice (Fig. 6*B*). However, the expression levels were significantly lower in *Cngb3*$^{-/-}$/*Nrl*$^{-/-}$ mice than in the *Nrl*$^{-/-}$ controls (Fig. 6*B*). Densitometric analysis showed that the expression levels of CNGA3, CAR, GNAT2, and M-opsin in 6-month *Cngb3*$^{-/-}$/*Nrl*$^{-/-}$ mice were reduced by about 40, 70, 65, and 65%, respectively, compared with those in age-matched *Nrl*$^{-/-}$ mice (Fig. 6*B*). Thus, CNGB3 deficiency leads to age-dependent impairment of cone function and cone degeneration. We also examined CNGB1a expression in *Cngb3*$^{-/-}$/*Nrl*$^{-/-}$ retinas to address the possibility that CNGB1a contributes to the observed cone light response. As we reported previously (22), CNGB1a was not detected in *Nrl*$^{-/-}$ retinas. Similarly, no CNGB1a immunoreactivity was detected in *Cngb3*$^{-/-}$/*Nrl*$^{-/-}$ retinas in contrast to its robust expression in wild-type and *Cngb3*$^{-/-}$ retinas (Fig. 6*C*). Hence, the residual cone response is unlikely contributed by the rod channel B subunit.

Enhanced Resistance to Proteolysis of the CNGA3 Channel Complexes—The susceptibility of a protein complex to proteolysis is an indication of the protein folding and conformational states (38, 42, 52). We used limited tryptic cleavage analysis to evaluate the channel complex conformation and folding states. Retinal membrane extracts of *Nrl*$^{-/-}$ and *Cngb3*$^{-/-}$/*Nrl*$^{-/-}$ mice were incubated with trypsin-TPCK (2.5 μg/ml) for 0, 0.5, 2, or 5 min. The digested products were analyzed by Western blotting analysis using anti-CNGA3 and anti-CNGB3. Under the given experimental conditions, CNGA3 in *Nrl*$^{-/-}$ retinas was substantially digested. In contrast, under the same experimental conditions, a significant amount of CNGA3 in *Cngb3*$^{-/-}$/*Nrl*$^{-/-}$ retinas was spared from tryptic digestion (Fig. 7*A*). After 2 min of trypsin exposure, the amount of undigested CNGA3 in *Cngb3*$^{-/-}$/*Nrl*$^{-/-}$ retinas remained almost unchanged from the initial level, whereas the amount of undi-

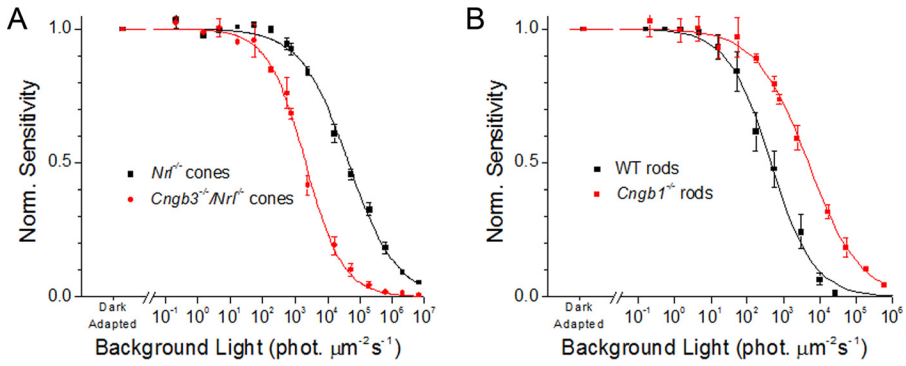

FIGURE 5. **Altered background light adaptation and functional range in *Cngb3*$^{-/-}$/*Nrl*$^{-/-}$ retinas.** Transretinal ERG recordings were performed in retinas from P30 *Nrl*$^{-/-}$, *Cngb3*$^{-/-}$/*Nrl*$^{-/-}$, wild-type (*WT*), and *Cngb1*$^{-/-}$ mice. The photosensitivity under increasing background light was plotted and fitted with the Weber-Fechner function. Shown are the normalized (*Norm.*) background adaptation curves in response to background light of increasing intensities recorded from cones from *Nrl*$^{-/-}$ and *Cngb3*$^{-/-}$/*Nrl*$^{-/-}$ mice (*A*) and rods from wild-type and *Cngb1*$^{-/-}$ mice (*B*). *Solid lines* represent the fit of the data with the Weber-Fechner function (see "Experimental Procedures" for details). *Error bars* represent S.E. *phot.*, photons.

gested CNGA3 was reduced by about 80% in *Nrl*$^{-/-}$ retinas (Fig. 7*B*). Similarly, CNGB3 immunoreactivity diminished after 2 min of trypsin exposure. Thus, mutant homomeric CNGA3 channels were more resistant to proteolytic cleavage than the native heteromeric CNGA3/CNGB3 cone channels. It is worth noting that the anti-CNGB3 and anti-CNGA3 antibodies used are peptide antibodies generated against peptides corresponding to the specific regions of the proteins (22, 34). We anticipate that these antibodies recognize both the linear epitope and the conformational epitope and may preferably recognize the linear epitope because the activity of these antibodies was verified with ELISA assays in which the specific linear peptides were used. The limited tryptic digestion will break down the channel subunits to small fragments/peptides based on the positions of the amino acid residues lysine (Lys) and arginine (Arg). Because both Lys and Arg residues are present in the antibody epitope, an effective tryptic digestion will interfere with the recognition of the channel protein (and the digested fragments) by the antibody.

Altered Velocity Sedimentation Profile of the CNGA3 Channel Complexes—Sedimentation velocity is commonly used to estimate the conformation, shape, and density of a protein complex (38, 43, 53). We used this approach to assess the buoyant density and conformation of the channel complexes. The Triton X-100-solubilized retinal membrane protein extracts prepared from *Cngb3*$^{-/-}$/*Nrl*$^{-/-}$ and *Nrl*$^{-/-}$ mice were separated in 5–20% (w/w) sucrose gradients, and the fractionated gradients were then assayed by Western blotting analysis with anti-CNGA3 antibody. As shown in Fig. 8*A*, although the overall sedimentation profiles between *Cngb3*$^{-/-}$/*Nrl*$^{-/-}$ and *Nrl*$^{-/-}$ mice were not drastically different, *Cngb3*$^{-/-}$/*Nrl*$^{-/-}$ retinas showed some distinction. CNGA3 immunoreactivity was nearly evenly detected in Fractions 5–9 from *Nrl*$^{-/-}$ retinas (Fig. 8*B*). However, more abundant CNGA3 immunoreactivity was detected in the lower buoyant density fractions in *Cngb3*$^{-/-}$/*Nrl*$^{-/-}$ retinas (Fractions 5 and 6) compared with higher buoyant density fractions (Fractions 7–9; Fig. 8*B*). These results suggest that the CNGA3 channels lacking CNGB3 tend to be resolved more abundantly in the lower buoyant density fractions compared with the results from CNGA3/CNGB3 channels.

Enhanced Circular Dichroism Spectral Profile Alterations of the CNGA3 C Termini in Response to cGMP—CD spectral analysis is an approach for monitoring conformational changes in a peptide or protein upon binding of its ligand (54). Binding of cGMP to the cyclic nucleotide-binding domains at the C termini of CNGA3 (CNGA3-C) and CNGB3 (CNGB3-C) and the subsequent conformational change are the critical step of the channel activation. We have shown the concentration-dependent reduction of the negative ellipticity of the CNGA3-C upon addition of 8-pCPT-cGMP (41). The current work compared the CD spectra between CNGA3-C and CNGA3-C/CNGB3-C. The CD spectra of CNGA3-C, CNGB3-C, and CNGA3-C/CNGB3-C were similar in the absence of 8-pCPT-cGMP. Upon addition of 8-pCPT-cGMP, CNGA3-C and CNGB3-C show an overall decrease in ellipticity with major negative peaks at 208 and 222 nm. However, the negative peak at 222 nm is significantly diminished upon addition of 8-pCPT-cGMP to CNGA3-C/CNGB3-C (Fig. 9). Hence, CNGB3 appears to affect ligand binding and/or conformational change of the channel in response to cGMP. Contributions of GST were subtracted from the spectra of GST-CNGA3-C and GST-CNGB3-C to obtain signal due to the C termini alone. As reported previously (41), GST showed no spectral changes upon addition of 8-pCPT-cGMP (Fig. 9).

Discussion

CNGB3 mutation is the main cause for human achromatopsia, but the role of CNGB3 in cones is not well understood. The major challenge in studying cone pathophysiology and cone protein biochemistry is the sparse population of cones in the rod-dominant mammalian retina. One approach for overcoming this issue has been using the all-cone retina of *Nrl*$^{-/-}$ mice. However, it is important to verify that the phenotype in the double *Cngb3*$^{-/-}$/*Nrl*$^{-/-}$ knock-out mice mimics that in the single *Cngb3*$^{-/-}$ knock-out mice to establish that the double knock-out line is a suitable model to study the defects caused by lack of CNGB3. Indeed, cones in the wild-type and *Nrl*$^{-/-}$ backgrounds do not always behave identically. For instance, *Cpfl1*/*Nrl*$^{-/-}$ mice show a different phenotype with recovery of cone function/ERG compared with *Cpfl1* mice (55). The difference in this case has been attributed to compensatory

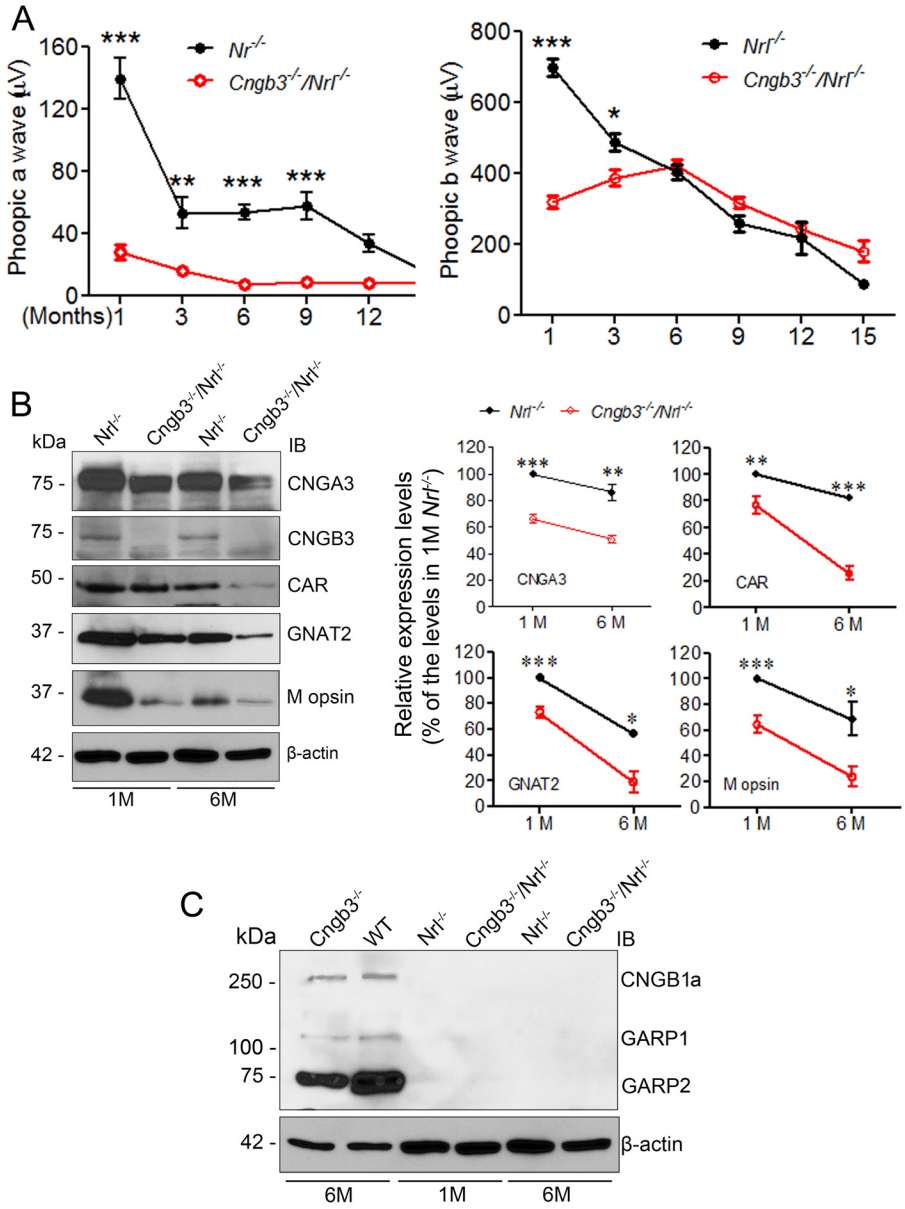

FIGURE 6. **Age-dependent reduction of the photopic a-wave but not the b-wave responses in *Cngb3*$^{-/-}$/*Nrl*$^{-/-}$ mice.** *A*, photopic ERG recordings were performed in *Cngb3*$^{-/-}$/*Nrl*$^{-/-}$ and *Nrl*$^{-/-}$ mice at varying ages between 1 and 15 months. Shown are the photopic a-wave and b-wave amplitudes in these mice. Data are represented as mean ± S.E. of measurements from five to eight mice. *B*, reduced expression levels of cone proteins in *Cngb3*$^{-/-}$/*Nrl*$^{-/-}$ retinas compared with those in *Nrl*$^{-/-}$ retinas. Shown are representative images of Western blotting detections of CNGA3, CNGB3, CAR, M-opsin, and GNAT2 in *Nrl*$^{-/-}$ and *Cngb3*$^{-/-}$/*Nrl*$^{-/-}$ mice at 1 (*1M*) and 6 months (*6M*) (*left panel*) and the corresponding densitometric analyses (*right panel*). Data are represented as mean ± S.E. of three assays using retinas from five to six mice. *C*, absence of CNGB1a expression in *Cngb3*$^{-/-}$/*Nrl*$^{-/-}$ and *Nrl*$^{-/-}$ retinas. Shown are representative images of Western blotting detection of CNGB1a expression in wild-type (*WT*), *Cngb3*$^{-/-}$, *Nrl*$^{-/-}$, and *Cngb3*$^{-/-}$/*Nrl*$^{-/-}$ mice at 1 and 6 months of age. Two-way analysis of variance was used to evaluate significance of difference between two genotypes at different ages (*, $p < 0.05$; **, $p < 0.01$; ***, $p < 0.001$). *Error bars* represent S.E. *IB*, immunoblotting.

expression of the rod PDE6 subunit (55). Another example is the *Rds*$^{-/-}$/*Nrl*$^{-/-}$ line. *Rds*$^{-/-}$ mice display no cone ERG response, whereas *Rds*$^{-/-}$/*Nrl*$^{-/-}$ mice show recovered cone ERG (31). Here, we first established that the basic phenotype (expression of CNGA3 and photopic ERG responses) in *Cngb3*$^{-/-}$/*Nrl*$^{-/-}$ mice is comparable with that in *Cngb3*$^{-/-}$ mice reported previously (23, 25). This allowed us to use the cone-dominant *Cngb3*$^{-/-}$/*Nrl*$^{-/-}$ mice to study the functional and biochemical role of CNGB3 in cones. The present work identified several functional defects and biochemical alterations of cones/CNGA3 channels lacking CNGB3 that enhance our understanding of the role of CNGB3 in cones.

CNGA3 Homomeric Channels Lacking CNGB3 Are Functional in Cones and Contribute to the Residual Cone Light Response—Similar to findings from *Cngb3*$^{-/-}$ mice (23, 25), *Cngb3*$^{-/-}$/*Nrl*$^{-/-}$ mice retained a residual cone light response. This was shown by ERG recordings both *in vivo* and *ex vivo*. It is apparent that the residual cone light response in CNGB3-deficient mice is mediated by the CNGA3 channels. This assumption is supported by the following experimental evidence obtained from the present study using *Cngb3*$^{-/-}$/*Nrl*$^{-/-}$ mice: 1) CNGA3 localization to the outer segment, 2) the presence of CNGA3 tetrameric complexes, and 3) the lack of CNGB1a in *Cngb3*$^{-/-}$/*Nrl*$^{-/-}$ retinas, which enables us to exclude the pos-

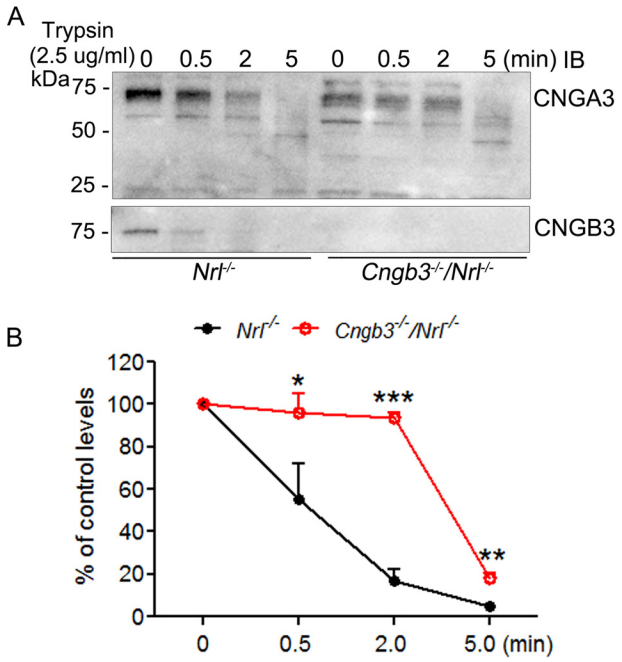

FIGURE 7. **CNGA3 channels lacking CNGB3 show enhanced resistance to proteolysis.** Retinal membrane extracts prepared from $Nrl^{-/-}$ and $Cngb3^{-/-}/Nrl^{-/-}$ mice were subjected to limited tryptic digestion at varying durations as indicated followed by Western blotting analysis using anti-CNGA3 and anti-CNGB3 antibodies. Shown are representative Western blot images (*A*) and the correlating densitometric analysis of CNGA3 detection (*B*). Data are represented as mean ± S.E. of three independent measurements from six to eight mice (*, $p < 0.05$; **, $p < 0.01$; ***, $p < 0.001$). *Error bars* represent S.E. *IB*, immunoblotting.

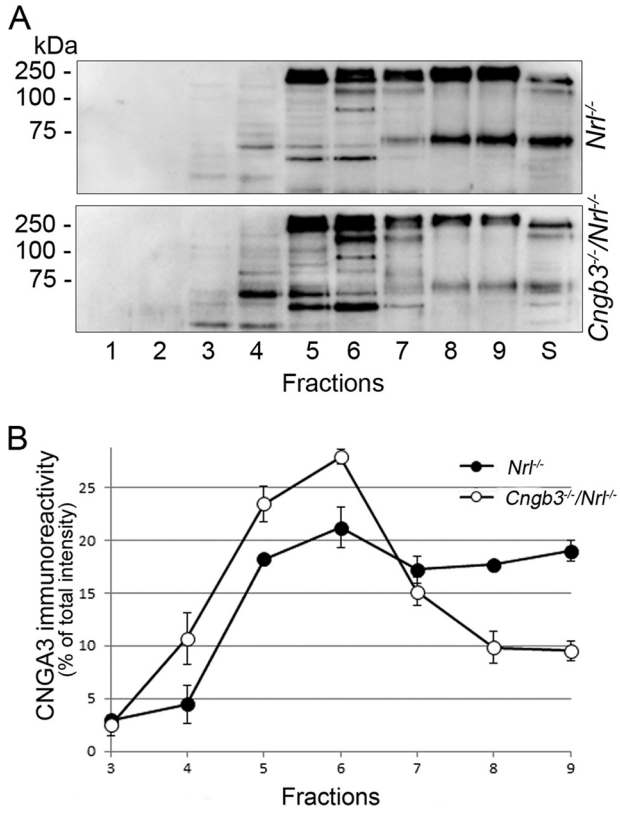

FIGURE 8. **CNGA3 channels lacking CNGB3 show altered velocity sedimentation profiles.** Triton X-100 extracts of $Nrl^{-/-}$ and $Cngb3^{-/-}/Nrl^{-/-}$ outer segment membranes were reduced and separated in 5–20% (w/w) sucrose gradients. Fractionated gradients were assayed by Western blotting analysis using anti-CNGA3. Shown are representative images of Western blotting detection of CNGA3 in the gradient fractions (*A*) and the plotting of the sedimentation profiles (*B*). Data are represented as mean ± S.E. of three independent measurements from eight to10 mice. *Error bars* represent S.E.

sibility of the compensative expression and contribution of CNGB1a in cones lacking CNGB3. Consistent with this notion, heterologous expression studies have shown that the CNGA3 homomeric channels in cultured cells are functional but display several distinct properties, including sensitivity to cGMP, cAMP, calcium channel blocker L-*cis*-diltiazem, and extracellular Ca^{2+} levels, compared with the native channels/heteromeric channels (3, 16, 21). Here, we present experimental evidence showing that CNGA3 homomeric channels in mouse cones lacking CNGB3 can support phototransduction. However, the light responses mediated by CNGA3 homomeric channels are dramatically impaired. Similarly, the homomeric rod CNG channel and olfactory CNG channels have been shown previously to be functional *in vivo*. Mice with a deficiency of CNGB1, which is the modulatory subunit of the rod CNG channel (CNGB1a) and olfactory CNG channel (CNGB1b), showed a residual rod light response (26, 56) and a residual odor response (57), suggesting a function mediated by the CNGA1 channels in rods and CNGA2/CNGA4 channels in olfactory neurons.

Although its expression was dramatically reduced in $Cngb3^{-/-}/Nrl^{-/-}$ retinas in the absence of CNGB3, CNGA3 was able to travel and localize to the cone outer segments. A similar observation was reported in rod CNG channels. Although deletion of CNGB1 dramatically reduced CNGA1 expression in the rods, CNGA1 localized specifically to the rod outer segments, and there was no detected mislocalization or accumulation of CNGA1 in other retinal compartments (26, 56). These findings support the view that the B subunits of photoreceptor CNG channels are important for the expression level and stability of the A subunits; however, they are not essential for these processes and the function of the channel. In the absence of their respective B subunits, CNGA3 and CNGA1 can travel and localize to the outer segments where they respond to light stimulation. However, it cannot be ruled out that the B subunits act to facilitate channel transport to the outer segments as reported for the olfactory channel (57).

Chemical cross-linking experiments showed that CNGA3 can form a tetramer in the absence of CNGB3. However, the relative amount of CNGA3 tetramers was significantly reduced in $Cngb3^{-/-}/Nrl^{-/-}$ retinas compared with that in $Nrl^{-/-}$ retinas (7 *versus* 48%). The observed functional defects could be a consequence of the reduced CNGA3 quantity and the proportion of channel in its tetrameric form. It is likely that the CNGB3-deficient cones suffer from both the lack of CNGA3/CNGB3 heterotetramers and the reduced level of CNGA3 homotetramers. Of note, we detected relatively more abundant CNGA3 trimers in the $Cngb3^{-/-}/Nrl^{-/-}$ retinas compared with $Nrl^{-/-}$ controls. These observations are in line with the findings that the A subunits of CNG channel exist as trimers for incorporation of a single B subunit to assemble a 3A and 1B tetrameric complex (58). With multiple biochemical and biophysical approaches, it was shown that the formation of a parallel three-helix coiled-coil domain of the C-terminal leucine

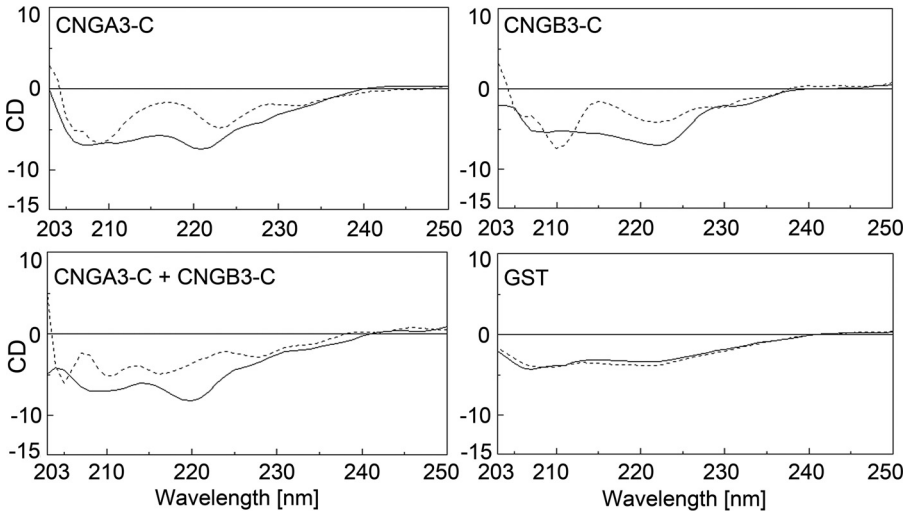

FIGURE 9. **Circular dichroism spectral profiles of CNGA3-C and CNGA3-C/CNGB3-C termini in response to cGMP.** The CD spectra of CNGA3-C and CNGA3-C/CNGB3-C upon addition of 8-pCPT-cGMP (100 μM) were obtained using GST-CNGA3-C and GST-CNGB3-C. Shown are representative CD spectral profiles of CNGA3-C, CNGB3-C, and CNGA3-C/CNGB3-C in response to 8-pCPT-cGMP. *Solid line*, no 8-pCPT-cGMP; *dashed line*, 100 μM 8-pCPT-cGMP. Contributions of GST were subtracted from the spectra of the fusion proteins to obtain signal due to the C termini alone. A representative CD spectral profile of GST in response to 8-pCPT-cGMP is included.

zipper region of CNGA1 subunits constrains the channel as a CNGA1 trimer followed by preferential incorporation of a single CNGB1 subunit (58). It was also shown that the x-ray crystal structures of the parallel three-helix coiled coil domains of CNGA1 and CNGA3 subunits were similar, suggesting a similar mechanism controlling the assembly of cone CNG channel complexes (58). It is worth mentioning that it is unlikely that the light response detected in *Cngb3*$^{-/-}$/*Nrl*$^{-/-}$ mice was mediated by the trimer complexes. Previous structural studies have demonstrated the functional CNG channel, like other members in the Eag-like K^+ channel family, to be a tetrameric complex, a structure essential for the formation of the ion-conducting pore (3, 17, 59).

In this work, we also examined the expression of CNGB1 and demonstrated the absence of CNGB1a in *Cngb3*$^{-/-}$/*Nrl*$^{-/-}$ mice. The lack of CNGB1a expression in *Cngb3*$^{-/-}$/*Nrl*$^{-/-}$ mice eliminated the possibility of a contribution by CNGB1a in the cone light response observed in *Cngb3*$^{-/-}$/*Nrl*$^{-/-}$ mice. Indeed, the compensatory expression of the rod counterpart in *Nrl*$^{-/-}$ cones when the cone protein is deleted has been reported (55).

CNGB3 Plays an Essential Role in Cone Light Response and Regulates Light Response Kinetics—Cngb3$^{-/-}$ and *Cngb3*$^{-/-}$/*Nrl*$^{-/-}$ mice display an impaired cone light response, demonstrated by Ganzfeld ERG and transretinal ERG recordings. There are several new findings obtained from evaluating *Cngb3*$^{-/-}$/*Nrl*$^{-/-}$ mice. 1) The reduced response amplitude was observed in both photopic a-wave and b-wave at all light stimulus intensities. The reductions were more profound in the a-wave responses compared with those in the b-wave responses, indicating a primary cone deficiency. 2) The cone light response was drastically impaired by deletion of CNGB3. However, the residual cone activity was sufficient to elicit a relatively ample and stable response of the secondary neurons, shown as better preserved photopic b-wave responses. 3) CNGB3 regulates cone light response sensitivity, and CNGB3 modulation is critical in relatively low light because the reduction in the ERG responses was more profound at lower light intensities compared with that at higher intensities. A similar phenotype was documented in *Cngb1*$^{-/-}$ mice, which show a dramatically reduced scotopic light response at lower light intensities compared with higher intensities (26, 56). 4) CNGB3-deficient mice displayed a reduced flicker response, which may reflect impaired temporal phototransduction processing. Consistent with this notion, CNGB3-deficient cones displayed abnormally slow response kinetics. The t_{rec} was increased by about 3-fold, and t_p was increased by about 1.6-fold in *Cngb3*$^{-/-}$/*Nrl*$^{-/-}$ mice, suggesting that CNGB3 is essential for normal cone light response kinetics. A similar functional role has been documented for CNGB1 in olfaction. The onset of the response to odorants was increased by about 4-fold in *Cngb1*$^{-/-}$ mice (57). 5) Cones in *Cngb3*$^{-/-}$/*Nrl*$^{-/-}$ mice showed a reduced functional range and an altered ability to adapt to background light. CNGB3 deletion resulted in about 8-fold desensitization in darkness and a profound shift of the adaptation curve to dimmer background light, suggesting a critical role of CNGB3 in the light adaptation and dynamic range of cones. In the present study, we also examined the background adaptation of rods in *Cngb1*$^{-/-}$ mice. Interestingly, the deletion of CNGB1 resulted in desensitization of rods in darkness and a corresponding shift of their adaptation curve to brighter light. Compared with CNGB1a deletion in rods, the deletion of CNGB3 in cones had more profound effects on the photoreceptor background adaptation and dynamic range. Hence, the regulation of background light adaptation is profoundly different in cones and rods, and CNGB3 and CNGB1a play distinct roles in these processes. Indeed, rod and cone CNG channels differ substantially in their cGMP sensitivity, Ca^{2+} permeation, channel structural features, and functional modulation (3, 60, 61). Rod CNG channel activity is tightly modulated by calmodulin (62–64). In contrast, the cone channel is regulated by a distinct calcium-binding protein, CNG-

modulin, via its interaction with CNGB3 (65, 66). The abnormally slow response recovery and the altered adaptation of cones lacking CNGB3 demonstrate the importance of CNGB3 in the calcium modulation of the channel function and in extending the dynamic range of cones to bright light. In addition, the reduction in the total channel number may contribute to the impairment of cone light response kinetics and recovery.

The Residual Cone Activity in CNGB3-deficient Cones Is Sufficient to Sustain the Stationary Responses of the Secondary Neurons in Aging Mice—We observed progressive reduction in the photopic a-wave response in $Cngb3^{-/-}/Nrl^{-/-}$ mice over the first 6 months after birth. This decline could be a consequence of both CNGB3 deficiency and NRL deficiency because the a-wave response in $Nrl^{-/-}$ mice also declines over age (31, 51) (see also Fig. 6*A*). In contrast to the a-wave response, the photopic b-wave response appeared to be more stable in $Cngb3^{-/-}/Nrl^{-/-}$ mice, similar to that observed in $Cngb3^{-/-}$ mice (25). The stationary nature of b-wave responses may reflect a compensatory regulation of the secondary neurons in response to the reduced photoreceptor function/input stimulation. The $Nrl^{-/-}$ background did not appear to affect this process in aging animals.

The analysis of cone protein expression levels showed age-dependent reduction in $Cngb3^{-/-}/Nrl^{-/-}$ mice, suggesting age-dependent cone degeneration. Because the age-dependent reduction in cone protein levels was observed in both $Cngb3^{-/-}/Nrl^{-/-}$ and $Nrl^{-/-}$ mice, the decline in $Cngb3^{-/-}/Nrl^{-/-}$ mice must be a cumulative consequence of the deficiencies of both CNGB3 and NRL. Consistent with this, the age-dependent reduction in cone protein levels in $Cngb3^{-/-}/Nrl^{-/-}$ mice appears to be more significant than that in $Cngb3^{-/-}$ mice. The reductions in 6-month $Cngb3^{-/-}/Nrl^{-/-}$ mice compared with the values in 1-month mice were in the range between 40 and 70% (Fig. 6*B*), whereas the reductions in 9-month $Cngb3^{-/-}$ mice were in the range between 30 and 50% (25). Together, our ERG and molecular studies indicate that the deletion of CNGB3 exacerbates the gradual cone loss in $Nrl^{-/-}$ mice.

CNGB3 Regulates Channel Biochemical Behaviors in Cones—CNGA3 channels display several biochemical features that are distinct from these of CNGA3/CNGB3 channels. CNGA3 channels were more abundantly resolved in lower buoyant densities in a sucrose gradient, which may indicate a reduced density of the channel complexes and/or an altered conformation. CNGA3 channels were also more resistant to limited proteolytic digestion under our experimental conditions, suggesting a weakened structural flexibility. The limited tryptic digestion broke down the channel subunits to small fragments/peptides and interfered with the recognition of the channel protein (and the digested fragments) by the antibody (the anti-CNGB3 and anti-CNGA3 antibodies used are peptide antibodies generated against peptides corresponding to the specific regions of the proteins). Thus, if the channel was less sensitive/more resistant to the limited tryptic digestion treatment, possibly associated with a reduced structural flexibility, it would allow a more abundant detection of the channel subunit following the reaction.

We further found that the C terminus of CNGA3 in the absence of the C terminus of CNGB3 is more responsive to cGMP compared with these in the presence of the C terminus of CNGB3, a result suggesting a regulation of the ligand binding and/or conformational change upon ligand binding by the C termini of CNGB3. The identified biochemical alterations may establish a structural basis for the observed distinctions in cone function mediated by the CNGA3 and CNGA3/CNGB3 channels.

In summary, CNGA3 channels lacking CNGB3 are functional in cones and contribute to the residual cone light response. However, CNGB3 deficiency results in several severe defects in cone function. These include reduced light response amplitudes, including photopic a-wave and b-wave responses; reduced light sensitivity; slowed response recovery that may impair temporal processing; and altered functional range. The residual cone activity in CNGB3-deficient cones is sufficient to sustain the stationary responses of the secondary neurons. Biochemically, CNGA3 channels show features that are distinct from those of CNGA3/CNGB3 channels in complex density, conformation, structural flexibility, and responsiveness to ligand binding. We conclude that the loss of modulation by CNGB3, along with the reduced channel number, contributes to the impairment of the cone light response in CNGB3-deficient cones.

Author Contributions—X.-Q. D., AT., K. K. R., and V. J. K. designed the study and wrote the manuscript. V. J. K. and S. J. P. contributed to study design and manuscript writing. A. T., H. M., J. X., M. H. E., M. L. S., K. K. R., J.-S. W., and V. J. K. performed experiments and analyzed data. S. J. P. provided the $Cngb1^{-/-}$ mouse line. All authors critically read and approved the final version of the manuscript.

Acknowledgments—We thank Drs. Anand Swaroop, Cheryl Craft, Muna Naash, and Robert Molday for providing the $Nrl^{-/-}$ mouse line and antibodies for M-opsin, cone arrestin, S-opsin, and CNGB1/glutamic acid-rich protein.

References

1. Cook, N. J., Molday, L. L., Reid, D., Kaupp, U. B., and Molday, R. S. (1989) The cGMP-gated channel of bovine rod photoreceptors is localized exclusively in the plasma membrane. *J. Biol. Chem.* **264,** 6996–6999
2. Kaupp, U. B., Niidome, T., Tanabe, T., Terada, S., Bönigk, W., Stühmer, W., Cook, N. J., Kangawa, K., Matsuo, H., Hirose, T., Miyata, T., and Numa, S. (1989) Primary structure and functional expression from complementary DNA of the rod photoreceptor cyclic GMP-gated channel. *Nature* **342,** 762–766
3. Kaupp, U. B., and Seifert, R. (2002) Cyclic nucleotide-gated ion channels. *Physiol. Rev.* **82,** 769–824
4. Biel, M., and Michalakis, S. (2009) Cyclic nucleotide-gated channels. *Handb. Exp. Pharmacol.* **191,** 111–136
5. Biel, M. (2009) Cyclic nucleotide-regulated cation channels. *J. Biol. Chem.* **284,** 9017–9021
6. Kohl, S., Marx, T., Giddings, I., Jägle, H., Jacobson, S. G., Apfelstedt-Sylla, E., Zrenner, E., Sharpe, L. T., and Wissinger, B. (1998) Total colourblindness is caused by mutations in the gene encoding the α-subunit of the cone photoreceptor cGMP-gated cation channel. *Nat. Genet.* **19,** 257–259
7. Wissinger, B., Gamer, D., Jägle, H., Giorda, R., Marx, T., Mayer, S., Tippmann, S., Broghammer, M., Jurklies, B., Rosenberg, T., Jacobson, S. G., Sener, E. C., Tatlipinar, S., Hoyng, C. B., Castellan, C., *et al.* (2001) CNGA3 mutations in hereditary cone photoreceptor disorders. *Am. J. Hum. Genet.* **69,** 722–737
8. Kohl, S., Baumann, B., Broghammer, M., Jägle, H., Sieving, P., Kellner, U.,

Spegal, R., Anastasi, M., Zrenner, E., Sharpe, L. T., and Wissinger, B. (2000) Mutations in the CNGB3 gene encoding the β-subunit of the cone photoreceptor cGMP-gated channel are responsible for achromatopsia (ACHM3) linked to chromosome 8q21. *Hum. Mol. Genet.* **9,** 2107–2116
9. Nishiguchi, K. M., Sandberg, M. A., Gorji, N., Berson, E. L., and Dryja, T. P. (2005) Cone cGMP-gated channel mutations and clinical findings in patients with achromatopsia, macular degeneration, and other hereditary cone diseases. *Hum. Mutat.* **25,** 248–258
10. Kohl, S., Varsanyi, B., Antunes, G. A., Baumann, B., Hoyng, C. B., Jägle, H., Rosenberg, T., Kellner, U., Lorenz, B., Salati, R., Jurklies, B., Farkas, A., Andreasson, S., Weleber, R. G., Jacobson, S. G., *et al.* (2005) CNGB3 mutations account for 50% of all cases with autosomal recessive achromatopsia. *Eur. J. Hum. Genet.* **13,** 302–308
11. Johnson, S., Michaelides, M., Aligianis, I. A., Ainsworth, J. R., Mollon, J. D., Maher, E. R., Moore, A. T., and Hunt, D. M. (2004) Achromatopsia caused by novel mutations in both CNGA3 and CNGB3. *J. Med. Genet.* **41,** e20
12. Sidjanin, D. J., Lowe, J. K., McElwee, J. L., Milne, B. S., Phippen, T. M., Sargan, D. R., Aguirre, G. D., Acland, G. M., and Ostrander, E. A. (2002) Canine CNGB3 mutations establish cone degeneration as orthologous to the human achromatopsia locus ACHM3. *Hum. Mol. Genet.* **11,** 1823–1833
13. Seddon, J. M., Hampson, E. C., Smith, R. I., and Hughes, I. P. (2006) Genetic heterogeneity of day blindness in Alaskan Malamutes. *Anim. Genet.* **37,** 407–410
14. Yeh, C. Y., Goldstein, O., Kukekova, A. V., Holley, D., Knollinger, A. M., Huson, H. J., Pearce-Kelling, S. E., Acland, G. M., and Komáromy, A. M. (2013) Genomic deletion of CNGB3 is identical by descent in multiple canine breeds and causes achromatopsia. *BMC Genet.* **14,** 27
15. Schön, C., Biel, M., and Michalakis, S. (2013) Gene replacement therapy for retinal CNG channelopathies. *Mol. Genet. Genomics* **288,** 459–467
16. Gerstner, A., Zong, X., Hofmann, F., and Biel, M. (2000) Molecular cloning and functional characterization of a new modulatory cyclic nucleotide-gated channel subunit from mouse retina. *J. Neurosci.* **20,** 1324–1332
17. Zagotta, W. N., and Siegelbaum, S. A. (1996) Structure and function of cyclic nucleotide-gated channels. *Annu. Rev. Neurosci.* **19,** 235–263
18. Okada, A., Ueyama, H., Toyoda, F., Oda, S., Ding, W. G., Tanabe, S., Yamade, S., Matsuura, H., Ohkubo, I., and Kani, K. (2004) Functional role of hCngb3 in regulation of human cone cng channel: effect of rod monochromacy-associated mutations in hCNGB3 on channel function. *Invest. Ophthalmol. Vis. Sci.* **45,** 2324–2332
19. Faillace, M. P., Bernabeu, R. O., and Korenbrot, J. I. (2004) Cellular processing of cone photoreceptor cyclic GMP-gated ion channels: a role for the S4 structural motif. *J. Biol. Chem.* **279,** 22643–22653
20. Bradley, J., Reisert, J., and Frings, S. (2005) Regulation of cyclic nucleotide-gated channels. *Curr. Opin. Neurobiol.* **15,** 343–349
21. Peng, C., Rich, E. D., Thor, C. A., and Varnum, M. D. (2003) Functionally important calmodulin-binding sites in both NH_2- and COOH-terminal regions of the cone photoreceptor cyclic nucleotide-gated channel CNGB3 subunit. *J. Biol. Chem.* **278,** 24617–24623
22. Matveev, A. V., Quiambao, A. B., Browning Fitzgerald, J., and Ding, X. Q. (2008) Native cone photoreceptor cyclic nucleotide-gated channel is a heterotetrameric complex comprising both CNGA3 and CNGB3: a study using the cone-dominant retina of $Nrl^{-/-}$ mice. *J. Neurochem.* **106,** 2042–2055
23. Ding, X. Q., Harry, C. S., Umino, Y., Matveev, A. V., Fliesler, S. J., and Barlow, R. B. (2009) Impaired cone function and cone degeneration resulting from CNGB3 deficiency: down-regulation of CNGA3 biosynthesis as a potential mechanism. *Hum. Mol. Genet.* **18,** 4770–4780
24. Thapa, A., Morris, L., Xu, J., Ma, H., Michalakis, S., Biel, M., and Ding, X. Q. (2012) Endoplasmic reticulum stress-associated cone photoreceptor degeneration in cyclic nucleotide-gated channel deficiency. *J. Biol. Chem.* **287,** 18018–18029
25. Xu, J., Morris, L., Fliesler, S. J., Sherry, D. M., and Ding, X. Q. (2011) Early-onset, slow progression of cone photoreceptor dysfunction and degeneration in CNG channel subunit CNGB3 deficiency. *Invest. Ophthalmol. Vis. Sci.* **52,** 3557–3566
26. Zhang, Y., Molday, L. L., Molday, R. S., Sarfare, S. S., Woodruff, M. L., Fain, G. L., Kraft, T. W., and Pittler, S. J. (2009) Knockout of GARPs and the β-subunit of the rod cGMP-gated channel disrupts disk morphogenesis and rod outer segment structural integrity. *J. Cell Sci.* **122,** 1192–1200
27. Mears, A. J., Kondo, M., Swain, P. K., Takada, Y., Bush, R. A., Saunders, T. L., Sieving, P. A., and Swaroop, A. (2001) Nrl is required for rod photoreceptor development. *Nat. Genet.* **29,** 447–452
28. Ma, H., Thapa, A., Morris, L. M., Michalakis, S., Biel, M., Frank, M. B., Bebak, M., and Ding, X. Q. (2013) Loss of cone cyclic nucleotide-gated channel leads to alterations in light response modulating system and cellular stress response pathways: a gene expression profiling study. *Hum. Mol. Genet.* **22,** 3906–3919
29. Daniele, L. L., Lillo, C., Lyubarsky, A. L., Nikonov, S. S., Philp, N., Mears, A. J., Swaroop, A., Williams, D. S., and Pugh, E. N., Jr. (2005) Cone-like morphological, molecular, and electrophysiological features of the photoreceptors of the Nrl knockout mouse. *Invest. Ophthalmol. Vis. Sci.* **46,** 2156–2167
30. Zhu, X., Brown, B., Li, A., Mears, A. J., Swaroop, A., and Craft, C. M. (2003) GRK1-dependent phosphorylation of S and M opsins and their binding to cone arrestin during cone phototransduction in the mouse retina. *J. Neurosci.* **23,** 6152–6160
31. Farjo, R., Skaggs, J. S., Nagel, B. A., Quiambao, A. B., Nash, Z. A., Fliesler, S. J., and Naash, M. I. (2006) Retention of function without normal disc morphogenesis occurs in cone but not rod photoreceptors. *J. Cell Biol.* **173,** 59–68
32. Kunchithapautham, K., Coughlin, B., Crouch, R. K., and Rohrer, B. (2009) Cone outer segment morphology and cone function in the $Rpe65^{-/-}$/$Nrl^{-/-}$ mouse retina are amenable to retinoid replacement. *Invest. Ophthalmol. Vis. Sci.* **50,** 4858–4864
33. Parker, R., Wang, J. S., Kefalov, V. J., and Crouch, R. K. (2011) Interphotoreceptor retinoid-binding protein as the physiologically relevant carrier of 11-*cis*-retinol in the cone visual cycle. *J. Neurosci.* **31,** 4714–4719
34. Ding, X. Q., Fitzgerald, J. B., Matveev, A. V., McClellan, M. E., and Elliott, M. H. (2008) Functional activity of photoreceptor cyclic nucleotide-gated channels is dependent on the integrity of cholesterol- and sphingolipid-enriched membrane domains. *Biochemistry* **47,** 3677–3687
35. Ma, H., Butler, M. R., Thapa, A., Belcher, J., Yang, F., Baehr, W., Biel, M., Michalakis, S., and Ding, X. Q. (2015) cGMP/protein kinase G signaling suppresses inositol 1,4,5-trisphosphate receptor phosphorylation and promotes endoplasmic reticulum stress in photoreceptors of cyclic nucleotide-gated channel-deficient mice. *J. Biol. Chem.* **290,** 20880–20892
36. Xu, J., Morris, L., Thapa, A., Ma, H., Michalakis, S., Biel, M., Baehr, W., Peshenko, I. V., Dizhoor, A. M., and Ding, X. Q. (2013) cGMP accumulation causes photoreceptor degeneration in CNG channel deficiency: evidence of cGMP cytotoxicity independently of enhanced CNG channel function. *J. Neurosci.* **33,** 14939–14948
37. Weitz, D., Ficek, N., Kremmer, E., Bauer, P. J., and Kaupp, U. B. (2002) Subunit stoichiometry of the CNG channel of rod photoreceptors. *Neuron* **36,** 881–889
38. Ding, X. Q., Nour, M., Ritter, L. M., Goldberg, A. F., Fliesler, S. J., and Naash, M. I. (2004) The R172W mutation in peripherin/rds causes a cone-rod dystrophy in transgenic mice. *Hum. Mol. Genet.* **13,** 2075–2087
39. Vinberg, F., Kolesnikov, A. V., and Kefalov, V. J. (2014) *Ex vivo* ERG analysis of photoreceptors using an *in vivo* ERG system. *Vision Res.* **101,** 108–117
40. Wang, J. S., Nymark, S., Frederiksen, R., Estevez, M. E., Shen, S. Q., Corbo, J. C., Cornwall, M. C., and Kefalov, V. J. (2014) Chromophore supply rate-limits mammalian photoreceptor dark adaptation. *J. Neurosci.* **34,** 11212–11221
41. Matveev, A. V., Fitzgerald, J. B., Xu, J., Malykhina, A. P., Rodgers, K. K., and Ding, X. Q. (2010) The disease-causing mutations in the carboxyl terminus of the cone cyclic nucleotide-gated channel CNGA3 subunit alter the local secondary structure and interfere with the channel active conformational change. *Biochemistry* **49,** 1628–1639
42. Nakamoto, R. K., Verjovski-Almeida, S., Allen, K. E., Ambesi, A., Rao, R., and Slayman, C. W. (1998) Substitutions of aspartate 378 in the phosphorylation domain of the yeast PMA1 H^+-ATPase disrupt protein folding and biogenesis. *J. Biol. Chem.* **273,** 7338–7344
43. Goldberg, A. F., Fales, L. M., Hurley, J. B., and Khattree, N. (2001) Folding and subunit assembly of photoreceptor peripherin/rds is me-

diated by determinants within the extracellular/intradiskal EC2 domain: implications for heterogeneous molecular pathologies. *J. Biol. Chem.* **276,** 42700–42706
44. Peachey, N. S., Goto, Y., al-Ubaidi, M. R., and Naash, M. I. (1993) Properties of the mouse cone-mediated electroretinogram during light adaptation. *Neurosci. Lett.* **162,** 9–11
45. Raz-Prag, D., Ayyagari, R., Fariss, R. N., Mandal, M. N., Vasireddy, V., Majchrzak, S., Webber, A. L., Bush, R. A., Salem, N., Jr., Petrukhin, K., and Sieving, P. A. (2006) Haploinsufficiency is not the key mechanism of pathogenesis in a heterozygous Elovl4 knockout mouse model of STGD3 disease. *Invest. Ophthalmol. Vis. Sci.* **47,** 3603–3611
46. Kondo, M., and Sieving, P. A. (2001) Primate photopic sine-wave flicker ERG: vector modeling analysis of component origins using glutamate analogs. *Invest. Ophthalmol. Vis. Sci.* **42,** 305–312
47. Qian, H., Shah, M. R., Alexander, K. R., and Ripps, H. (2008) Two distinct processes are evident in rat cone flicker ERG responses at low and high temporal frequencies. *Exp. Eye Res.* **87,** 71–75
48. Wang, J. S., Estevez, M. E., Cornwall, M. C., and Kefalov, V. J. (2009) Intra-retinal visual cycle required for rapid and complete cone dark adaptation. *Nat. Neurosci.* **12,** 295–302
49. Kolesnikov, A. V., and Kefalov, V. J. (2012) Transretinal ERG recordings from mouse retina: rod and cone photoresponses. *J. Vis. Exp.* 3424
50. Daiger, S. P., Sullivan, L. S., and Bowne, S. J. (2013) Genes and mutations causing retinitis pigmentosa. *Clin. Genet.* **84,** 132–141
51. Roger, J. E., Ranganath, K., Zhao, L., Cojocaru, R. I., Brooks, M., Gotoh, N., Veleri, S., Hiriyanna, A., Rachel, R. A., Campos, M. M., Fariss, R. N., Wong, W. T., and Swaroop, A. (2012) Preservation of cone photoreceptors after a rapid yet transient degeneration and remodeling in cone-only $Nrl^{-/-}$ mouse retina. *J. Neurosci.* **32,** 528–541
52. Ding, X. Q., Pinon, D. I., Furse, K. E., Lybrand, T. P., and Miller, L. J. (2002) Refinement of the conformation of a critical region of charge-charge interaction between cholecystokinin and its receptor. *Mol. Pharmacol.* **61,** 1041–1052
53. Chakraborty, D., Ding, X. Q., Conley, S. M., Fliesler, S. J., and Naash, M. I. (2009) Differential requirements for retinal degeneration slow intermolecular disulfide-linked oligomerization in rods versus cones. *Hum. Mol. Genet.* **18,** 797–808
54. Siligardi, G., and Hussain, R. (1998) Biomolecules interactions and competitions by non-immobilised ligand interaction assay by circular dichroism. *Enantiomer* **3,** 77–87
55. Kolandaivelu, S., Chang, B., and Ramamurthy, V. (2011) Rod phosphodiesterase-6 (PDE6) catalytic subunits restore cone function in a mouse model lacking cone PDE6 catalytic subunit. *J. Biol. Chem.* **286,** 33252–33259
56. Hüttl, S., Michalakis, S., Seeliger, M., Luo, D. G., Acar, N., Geiger, H., Hudl, K., Mader, R., Haverkamp, S., Moser, M., Pfeifer, A., Gerstner, A., Yau, K. W., and Biel, M. (2005) Impaired channel targeting and retinal degeneration in mice lacking the cyclic nucleotide-gated channel subunit CNGB1. *J. Neurosci.* **25,** 130–138
57. Michalakis, S., Reisert, J., Geiger, H., Wetzel, C., Zong, X., Bradley, J., Spehr, M., Hüttl, S., Gerstner, A., Pfeifer, A., Hatt, H., Yau, K. W., and Biel, M. (2006) Loss of CNGB1 protein leads to olfactory dysfunction and subciliary cyclic nucleotide-gated channel trapping. *J. Biol. Chem.* **281,** 35156–35166
58. Shuart, N. G., Haitin, Y., Camp, S. S., Black, K. D., and Zagotta, W. N. (2011) Molecular mechanism for 3:1 subunit stoichiometry of rod cyclic nucleotide-gated ion channels. *Nat. Commun.* **2,** 457
59. Liu, D. T., Tibbs, G. R., and Siegelbaum, S. A. (1996) Subunit stoichiometry of cyclic nucleotide-gated channels and effects of subunit order on channel function. *Neuron* **16,** 983–990
60. Picones, A., and Korenbrot, J. I. (1995) Permeability and interaction of Ca^{2+} with cGMP-gated ion channels differ in retinal rod and cone photoreceptors. *Biophys. J.* **69,** 120–127
61. Rebrik, T. I., and Korenbrot, J. I. (1998) In intact cone photoreceptors, a Ca^{2+}-dependent, diffusible factor modulates the cGMP-gated ion channels differently than in rods. *J. Gen. Physiol.* **112,** 537–548
62. Trudeau, M. C., and Zagotta, W. N. (2004) Dynamics of Ca^{2+}-calmodulin-dependent inhibition of rod cyclic nucleotide-gated channels measured by patch-clamp fluorometry. *J. Gen. Physiol.* **124,** 211–223
63. Trudeau, M. C., and Zagotta, W. N. (2002) Mechanism of calcium/calmodulin inhibition of rod cyclic nucleotide-gated channels. *Proc. Natl. Acad. Sci. U.S.A.* **99,** 8424–8429
64. Weitz, D., Zoche, M., Müller, F., Beyermann, M., Körschen, H. G., Kaupp, U. B., and Koch, K. W. (1998) Calmodulin controls the rod photoreceptor CNG channel through an unconventional binding site in the N-terminus of the β-subunit. *EMBO J.* **17,** 2273–2284
65. Rebrik, T. I., Botchkina, I., Arshavsky, V. Y., Craft, C. M., and Korenbrot, J. I. (2012) CNG-modulin: a novel Ca-dependent modulator of ligand sensitivity in cone photoreceptor cGMP-gated ion channels. *J. Neurosci.* **32,** 3142–3153
66. Korenbrot, J. I., Mehta, M., Tserentsoodol, N., Postlethwait, J. H., and Rebrik, T. I. (2013) EML1 (CNG-modulin) controls light sensitivity in darkness and under continuous illumination in zebrafish retinal cone photoreceptors. *J. Neurosci.* **33,** 17763–17776